Mohammed, S. Afshan. (2022) Modelling and design of stainless steel hollow section beam-column members in fire. **International Journal of Steel Structures.** https://doi.org/10.1007/s13296-022-

Modelling and design of stainless steel hollow section beam-column members in fire

A. Mohammed [a*], S. Afshan [b]

[a] Department of Civil and Environmental Engineering, Brunel University London, London, U.K.
[b] Faculty of Engineering and Physical Sciences, University of Southampton, Southampton, U.K.

Abstract

This paper presents the results of a comprehensive numerical modelling study on the performance and design of stainless steel square, rectangular and circular hollow section beam-column members subjected to axial compressive load and uniform bending moment at elevated temperatures. The numerical results generated have been used to assess the level of safety and predictive accuracy of the combined axial compressive load and bending moment resistances of hollow section stainless steel beam-column members determined from EN 1993-1-2 fire design rules. New design recommendations, which include: (i) new elevated temperature flexural buckling formulation for SHS, RHS and CHS stainless steel columns to obtain accurate predictions of the pure compression capacity and (ii) new combined loading interaction factors for the combined axial load and bending moment interaction equations, are proposed. The higher accuracy and improved reliability of the proposals for predicting the load-carrying capacity of stainless steel SHS, RHS and CHS beam-column members in fire is demonstrated through numerical comparisons and reliability assessments.

Keywords: Beam-column; Elevated temperature, Fire design; Numerical modelling; Reliability; Stainless steel.

1. Introduction

Stainless steels are used in a diverse range of structural applications that take advantage of the unique durability and strength characteristics that are offered by the variety of available stainless steel grades. The behaviour, analysis and design of stainless steel structures at both room and elevated temperature conditions have been the subject of a number of experimental and numerical modelling research studies in recent years, which have enabled the development and expansion of dedicated structural design guidance rules worldwide e.g. EN 1993-1-4 [1] in Europe, AS/NZS 4673:2001 [2] in Australia and New Zealand, AISC Design Guide 27 [3] and ASCE/SEI-8 [4] in the United States and CECS-410 [5] in China. The performance of stainless steel structures at elevated temperatures has been of particular importance as the structural elements are often left without passive fire protection and need to show adequate fire resistance. The behaviour of unprotected stainless steel structural members exposed to high temperatures has been investigated

at material level, member level and system level by a number of researchers, an overview of which is provided hereafter.

Chen and Young [6] proposed a series of equations for predicting the yield stress, elastic modulus, ultimate tensile stress and strain at the ultimate tensile stress of stainless steel, covering the EN 1.4462, 1.4301 and 1.4571 grades, at elevated temperature based on the results of isothermal and anisothermal tests. In addition, a stress-strain model for stainless steel at elevated temperature was also developed, whereby the compound Ramberg-Osgood material model [7] was recalibrated for elevated temperatures. Gardner et al. [8] proposed revised strength and stiffness reduction factors at elevated temperatures for a range of stainless steel grades, based on examination of all the then available reported test data. Reduction factors rationalised on the basis of grouping grades that exhibit similar elevated temperature properties were also proposed. In addition, a material model for the continuous prediction of the stress-strain response by means of a modified Ramberg-Osgood formulation, utilising the stress at 2% total strain, was proposed. It was found that the proposed model is more accurate, when compared to test results, and simpler to apply than the EN 1993-1-2 [9] elevated temperature stress-strain model. Huang and Young [10] carried out a test programme to examine the elevated temperature material properties of a relatively new cold-formed lean-duplex (EN 1.4162) stainless steel grade and proposed new strength and stiffness reduction factors. In the Design Manual for Structural Stainless Steel [11] stainless steels with similar elevated temperature properties have been put into seven groups and reduction factors which apply to these groups are provided. The studies on the stainless steel material behaviour at elevated temperature discussed above have shown that it offers better retention of strength and stiffness that carbon steel due to the variation in the microstructure and alloying content between the materials especially at the important temperature range of 550-750 ºC, as illustrated in Figure 1.

Experimental and numerical modelling investigations on stainless steel structural members have been carried out to investigate the influence of stainless steels' distinct mechanical and thermal properties on the response of its members and to assess the suitability of the existing fire design codes. The elevated temperature flexural buckling behaviour and design of austenitic (EN 1.4301) stainless steel hollow box section columns have been studied by Ng and Gardner [12] and Fan et al. [13] where in each, the EN 1993-1-2 buckling curve was assessed and a modified version of which was proposed that more accurately fitted the numerically generated structural performance data. Huang and Young [14] carried out a numerical modelling analysis on cold-formed lean duplex stainless steel columns subjected to elevated temperatures and assessed the accuracy of

the existing codified design provisions, including those of AS/NZS, EC3 and ASCE, and the newly proposed design methods, including the Continuous Strength Method and the Direct Strength Method. Tondini et al [15] conducted anisothermal fire tests on ferritic (EN 1.4301) stainless steel hollow box section columns, which had not been investigated previously. Lopes et al. [16] studied the compression behaviour of stainless steel I-section columns in fire and proposed a new elevated temperature buckling curve formulation for their design, which was later extended to circular hollow section columns by Arrais et al. [17]. Huang and Young [18] investigated the structural performance of stainless steel lean duplex SHS and RHS beams at elevated temperatures and assessed the results against current codified design standards and proposed a modified direct strength method, which was shown to give reliable predictions for flexural beam members at elevated temperatures. More recently, Kucukler et al. and Xing et al. [19-20] also studied the flexural buckling behaviour of stainless steel I-section columns at elevated temperature and proposed a series of temperature dependent buckling curves which were calibrated against data from an extensive numerical parametric modelling programme covering austenitic, duplex and ferritic stainless steels. Huang et al. [21] investigated flexural buckling response and design of cold-formed austenitic, duplex, and lean duplex stainless steel SHS and RHS beam-columns elements in the minor axis at elevated temperature and proposed that the Australian/New Zealand Standard to be used for the fire design of cold-formed stainless steel RHS and SHS beam-columns, due to its reliable beam-column predictions. More recently the fire performance of stainless steel frame assemblies were investigated by Segura et al. [22], which building on the studies on restrained stainless steel structural columns [23] and beams [24] in fire, investigated the combined effects of material degradation with temperature and the interaction between the individual frame elements on the fire resistance.

In this context, this paper makes a contribution to the state of the art on the behaviour of hollow section beam-columns made from austenitic, duplex and ferritic stainless steel in fire by examining the applicability of existing design guidance based on a large set of structural performance data, covering SHS, RHS (Major and Minor axis) and CHS hollow sections, generated through finite element analysis. The paper begins with an overview of the Eurocode 3 design guidance rules for steel beam-columns in fire, followed by the description of the developed finite element models and the validation results. The proposed beam-column design equations for stainless steel SHS, RHS and CHS in fire are then described. The details of the parametric study models used to generate the structural performance data for the assessment of the proposed design equations together with the results of the analysis and comparisons are presented.

2. Eurocode 3 design rules for beam-columns members in fire

In this section the Eurocode fire design expressions for stainless steel beam-column members under axial compressive load plus major and minor uniaxial bending are described. EN 1993-1-4 [1], which is the Eurocode 3 part with supplementary design guidelines for structures made of stainless steel, makes reference to the guideline in EN 1993-1-2 [9] for fire design provisions, where the design rules provided are mainly based on those developed for carbon steel structures. The current fire design expressions for stainless steel beam-columns under compressive axial load plus uniaxial bending in the major and minor axes are given in Eqs (1) and (2) for Class 1 and Class 2 cross-sections with and without lateral-torsional buckling (LTB), respectively and Eqs (3) and (4) for Class 3 cross-section with and without lateral-torsional buckling (LTB), respectively.

For axial load + Major axis bending + Minor axis bending (without LTB) – Class 1 and 2

$$\frac{N_{fi,Ed}}{\chi_{min,fi} A k_{y,\theta} f_y / \gamma_{M,fi}} + k_y \frac{M_{y,fi,Ed}}{W_{pl,y} k_{y,\theta} f_y / \gamma_{M,fi}} + k_z \frac{M_{z,fi,Ed}}{W_{pl,z} k_{y,\theta} f_y / \gamma_{M,fi}} \leq 1 \quad (1)$$

For Axial load + Major axis bending + Minor axis bending (with LTB) – Class 1 and 2

$$\frac{N_{fi,Ed}}{\chi_{z,fi} A k_{y,\theta} f_y / \gamma_{M,fi}} + k_{L.T.} \frac{M_{y,fi,Ed}}{\chi_{LT,fi} W_{pl,y} k_{y,\theta} f_y / \gamma_{M,fi}} + k_z \frac{M_{z,fi,Ed}}{W_{pl,z} k_{y,\theta} f_y / \gamma_{M,fi}} \leq 1 \quad (2)$$

For Axial load + Major axis bending + Minor axis bending (without LTB) – Class 3

$$\frac{N_{fi,Ed}}{\chi_{min,fi} A k_{y,\theta} f_y / \gamma_{M,fi}} + k_y \frac{M_{y,fi,Ed}}{W_{el,y} k_{y,\theta} f_y / \gamma_{M,fi}} + k_z \frac{M_{z,fi,Ed}}{W_{el,z} k_{y,\theta} f_y / \gamma_{M,fi}} \leq 1 \quad (3)$$

For Axial load + Major axis bending + Minor axis bending (with LTB) – Class 3

$$\frac{N_{fi,Ed}}{\chi_{z,fi} A k_{y,\theta} f_y / \gamma_{M,fi}} + k_{L.T.} \frac{M_{y,fi,Ed}}{\chi_{LT,fi} W_{el,y} k_{y,\theta} f_y / \gamma_{M,fi}} + k_z \frac{M_{z,fi,Ed}}{W_{el,z} k_{y,\theta} f_y / \gamma_{M,fi}} \leq 1 \quad (4)$$

The definition of symbols in Eqs (1)-(4) is as follows: $N_{fi,Ed}$, $M_{y,fi,Ed}$ and $M_{z,fi,Ed}$ are the design values for the axial load, major axis moment and minor axis moment in the fire situation, respectively, $\chi_{min,fi}$ is the smallest of reduction factors for flexural, torsional and torsional-flexural buckling at elevated temperature, $\chi_{z,fi}$ and $\chi_{LT,fi}$ are the reduction factors for minor axis flexural buckling and lateral torsional buckling at elevated temperature, respectively, A is the cross-sectional area, $k_{y,\theta}$ is the elevated temperature reduction factor for yield stress f_y, $\gamma_{M,fi}$ is the partial safety factor for member resistance in fire, k_y, $k_{L.T.}$, k_z are the combined loading interaction factors for elevated temperature.

The combined loading interaction factors at elevated temperature, k_y and k_z, are given by Eqs (5) and (6) for major and minor axes, respectively, where $\beta_{M,y}$ and $\beta_{M,z}$ are the equivalent uniform moment factors for the major and minor axes, respectively, $\chi_{y,fi}$ and $\chi_{z,fi}$ are the flexural buckling reduction factors for major and minor axes, respectively at elevated temperature and $\bar{\lambda}_{y,\theta}$ and $\bar{\lambda}_{z,\theta}$ are the non-dimensional member slenderness for major and minor axes, respectively at elevated temperature θ, which are defined by Eqs (7) and (8), where $\bar{\lambda}_y$ and $\bar{\lambda}_z$ are the respective member slendernesses at room temperature and $k_{E,\theta}$ is the stiffness reduction factor.

$$k_y = 1 - \frac{\mu_y N_{fi,Ed}}{\chi_{y,fi} A k_{y,\theta} f_y / \gamma_{M,fi}} \leq 3 \quad \text{with } \mu_y = (2\beta_{M,y} - 5)\,\bar{\lambda}_{y,\theta} + 0.44\beta_{M,y} + 0.29 \leq 0.8 \text{ with } \bar{\lambda}_{y,20} \leq 1.1 \tag{5}$$

$$k_z = 1 - \frac{\mu_z N_{fi,Ed}}{\chi_{z,fi} A k_{y,\theta} f_y / \gamma_{M,fi}} \leq 3 \quad \text{with } \mu_z = (1.2\beta_{M,z} - 3)\bar{\lambda}_{z,\theta} + 0.71\beta_{M,z} - 0.29 \leq 0.8 \tag{6}$$

$$\bar{\lambda}_{y,\theta} = \bar{\lambda}_y \left[\frac{k_{y,\theta}}{k_{E,\theta}}\right]^{0.5} \tag{7}$$

$$\bar{\lambda}_{z,\theta} = \bar{\lambda}_z \left[\frac{k_{z,\theta}}{k_{E,\theta}}\right]^{0.5} \tag{8}$$

3. Development and validation of numerical models

Numerical models for predicting the combined axial compressive load and uniform bending moment resistances of stainless steel beam-column members in fire were developed. This section describes the development and validation of the finite element (F.E.) models which are then used to generate the performance data required for the assessment of the existing design rules presented in Section 2 and the development and analysis of the proposed design method in Sections 4 and 5, respectively. The additional modelling assumption related to the parametric study models are further reported in Section 4.3.

3.1 Literature tests for validation

A selection of elevated and room temperature tests on stainless steel and carbon steel hollow section beam-column members were used for the validation of the F.E. models. A number of experimental test programmes on stainless steel beam-column SHS, RHS and CHS members at room temperature were conducted by Zhao et al. [25-26], the selection of which used for the

model validation herein is presented in Table 1, where e_y and e_z are the applied major and minor axes eccentricities, respectively, L is the member length and $N_{u,test}$ is the measured ultimate compressive load. Two tests on stainless steel SHS beam-column members at elevated temperature were carried out by Fan et al. [13] and are reported in Table 2. These tests had anisothermal loading, where the specimens were first loaded at room temperature to load N, which was then held constant, followed by temperature increase until failure was reached at critical specimen temperature θ_{test}, the measured values of which are reported in Table 2, where all other parameters are as previously defined. Owing to the limited number of stainless steel beam-column tests at elevated temperature, additional test data on carbon steel RHS beam-column members carried out by Pauli et al. [27] were also adopted for the validation of the models. Isothermal loading was employed for these tests, where the specimens were heated to a specified temperature θ, which was held constant, followed by an increase in the applied compressive load until failure at $N_{u,test}$ as reported in Table 3. Table 1, 2 and 3 presents the non-dimensional slenderness $\bar{\lambda}$.

3.2 Development of numerical models

The finite element analysis package ABAQUS was employed to develop the numerical models [28]. The shell element S4R was used to discretise the models. The size of the shell elements was based on the results of a mesh sensitivity study. For the SHS and RHS, an element size equal to the cross-section thickness was assigned to the flat regions of the sections, whilst a finer mesh of four elements were employed in the corner regions. For the CHS the element size was set equal to the cross-section thickness. The measured cross-section dimensions and length of the specimens were adopted, and suitable displacement and rotational constraints were applied at the model ends to mimic the test pinned boundary conditions. For columns and beam-column models with pinned end boundary conditions, all translational degrees of freedom, except axial displacement at the loaded end, were restrained (i.e. u_x=0, u_y=0 and $u_z \neq 0$) with the rotational degrees of freedom restrained at both ends, except that related to the plane of buckling (u_{Rx}=0, $u_{Ry} \neq 0$ and u_{Rz}=0 for buckling about y-y (major) axis and $u_{Rx} \neq 0$, u_{Ry}=0 and u_{Rz}=0 for buckling about z-z (minor) axis). Figure 2 illustrates the boundary condition for buckling about the major axis.

The measured room and elevated temperature stress-strain responses reported in the test programmes [13, 25-27] were used to define the material behaviour in ABAQUS in the form of true strain ε_T and true stress σ_T using the well-known relations $\varepsilon_T = \ln(1+\varepsilon_n)$ and $\sigma_T = \sigma_n (1+\varepsilon_n)$, where ε_n is the engineering strain and σ_n is the engineering stress. For beam-columns reported in [26], the measured corner material properties were adopted in the FE model. For Fan et al. [13]

beam-columns, the material properties used for the corner regions of the sections were not measured, and hence flat material properties were used, as the numerical study counterpart performed in [29]. Geometric imperfections, global and local, were included in the numerical models. The lowest form of the global and local imperfection was employed as an imperfection shape, extracted through a linear buckling analysis. The imperfection amplitudes were based on either measured or predicted values. Measured global imperfection amplitudes was employed for all the models, except for models of the tests in [25], where a value of $L/1000$, L being the length of the element, was adopted. For local imperfection amplitudes, the CHS was set at $t/10$, where t is the cross-section thickness of the CHS, as recommended in [30], and predictions from the Dawson and Walker model for the SHS and RHS, as recommended in [31].

Residual stresses are introduced into the cold-formed specimens during the production process, with a combination of membrane residual stresses from welding and through-thickness bending residual stresses due to cold-forming. Careful measurements [32] have shown the latter to be relatively insignificant in stainless steel hollow sections and largely swamped by the dominant bending residual stresses. Furthermore, the effect of the bending residual stresses is inherently present in the material stress-strain properties [32-33] since the residual stresses that are released during the cutting of the coupons (causing longitudinal curvature) are essentially reintroduced by straightening of the coupons during testing. This has been adopted in many studies [12,15,17,31,34] at room and elevated temperature. Residual stresses were not therefore explicitly introduced into the described models, but their influence was present in the material modelling. For the room temperature and the isothermal elevated temperature tests, the modified Riks method was used to solve the materially and geometrically nonlinear problem. For the anisothermal elevated temperature tests, general static analysis was performed in two steps which involved (1) application of a static concentric compressive load equal to the test load and (2) increasing the specimen temperature according to the test measured temperature-time curves until failure.

The measured specimen temperature-time data reported in [13] was utilised in the numerical models developed for the austenitic beam-columns in ABAQUS. Figure 3 illustrates the time-temperature curve used for the two beam-column SHS section having a 13.2mm and 23.8mm eccentricity [13] used for the numerical models.

3.3 Validation results

The comparison results for the F.E. ultimate load $N_{u,\,F.E.}$ and displacement at ultimate load $\delta_{u,\,F.E.}$ and the test ultimate load $N_{u,test}$ and displacement at ultimate load $\delta_{u,test}$ for the modelled room temperature tests [25-26] are presented in Table 1, giving a mean $N_{u,test}/N_{u,\,F.E.}$ and $\delta_{u,test}/\delta_{u,\,F.E.}$ of

0.98 and 0.99 with coefficients of variation (COV) of 0.02 and 0.05, respectively. Example test and F.E. load-deflection response curves are also shown in Figure 4, where the test and F.E. responses match closely. The predicted critical temperatures θ_{FE} for the modelled anisothermal elevated temperature tests [25] are reported in Table 2, where the mean and COV of $\theta_{FE}/\theta_{test}$ are 1.01 and 0.01, respectively. Figure 5 compares the axial displacement-time responses from the tests and F.E. for the SHS 120×120×4 when e_y = 13.2 mm. The predicted ultimate load and displacement at ultimate load for the modelled isothermal elevated temperature tests [27] are reported in Table 3, giving a mean $N_{u,test}/N_{u,\ F.E.}$ of 1.02 with a COV of 0.08 and mean $\delta_{u,test}/\delta_{u,\ F.E.}$ of 1.03 with a COV of 0.09. The comparison of the axial load-deformation response of the test and F.E. results are displayed in Figure 6, where it is shown that the models of capable of accurately tracing the load-deformation response. There are some relatively small discrepancies between the experimental and numerical values as well as the overall behaviour and these are most likely due to the differences in the geometric and imperfection values used in the model compared with the physical specimens, and also the use of idealised boundary conditions in the model. In addition, with fire testing, there are many factors and variables which can occur during the test, and these are not easy to measure or simulate accurately. Figure 7 compares typical test and FE failure modes for the modelled beam-columns, showing the models ability to capture the observed behaviours. The numerical modelling approach presented herein is therefore considered sufficient for performing numerical parametric modelling analysis.

4. Proposed design method and development

4.1 Combined axial load and bending moment interaction equations

As discussed in Section 2, the EN 1993-1-2 [9] design rules for stainless steel beam-column members in fire were simply taken as those for carbon steel beam-columns without rigorous verification. In addition, they are based on the flexural buckling curves in EN 1993-1-2 [9], which were shown in [34] to give inaccurate and unsafe predictions of the flexural buckling capacities of stainless steel hollow section columns in fire. Hence, to overcome these limitations, in this section, new design expressions for combined axial load and uniaxial major axis bending (without LTB) given by Eq. (9) and combined axial load and uniaxial minor axis bending (without LTB) given by Eq. (10) are proposed. These design expressions are of the same form as the EN 1993-1-2 [9] expressions, but employ the flexural buckling resistances from the flexural buckling curves proposed by the authors in [33], a summary of which is provided in Section 4.2, and incorporate the newly proposed combined loading interaction factors k_y and k_z calibrated on the basis of the numerical results of stainless steel beam-column members presented in Section 4.3 of this paper.

$$\frac{N_{fi,Ed}}{N_{b,y,Rd,fi}/\gamma_{M,fi}} + k_y \frac{M_{y,fi,Ed}}{M_{c,y,Rd,fi}/\gamma_{M,fi}} \leq 1 \quad (9)$$

$$\frac{N_{fi,Ed}}{N_{b,z,Rd,fi}/\gamma_{M,fi}} + k_z \frac{M_{z,fi,Ed}}{M_{c,z,Rd,fi}/\gamma_{M,fi}} \leq 1 \quad (10)$$

where $N_{b,y,Rd,fi}$ and $N_{b,z,Rd,fi}$ are the major and minor axes flexural buckling resistances in fire, respectively (obtained from the proposed method in [21]), $M_{c,y,Rd,fi}$ and $M_{c,z,Rd,fi}$ are the major and minor axes cross-section bending moment resistances in fire, k_y and k_z are the new proposed major and minor axes combined loading interaction factors, respectively and all other symbols are as previously defined.

4.2 Flexural buckling resistance

The flexural buckling formulation for the design of cold-formed stainless steel SHS, RHS and CHS columns derived in [34] are given by Eq. (11)-(13). In Eq. (11), χ_{fi} is the reduction factor for flexural buckling at elevated temperature for the concerned axis of buckling i.e. $\chi_{y,fi}$ for major axis and $\chi_{z,fi}$ for minor axis, A is the cross-sectional area, taken as the gross cross-sectional area for fully effective sections (Class 1-3) and the effective cross-sectional area for slender sections (Class 4), $k_{y,\theta}$ is the elevated temperature reduction factor for yield stress, taken as $k_{2,\theta}$ for fully effective sections (Class 1-3) and the $k_{0.2,\theta}$ for slender sections (Class 4) and $\gamma_{M,fi}$ is the partial safety factor for member resistance in fire. In Eq. (12), α is the imperfection parameter defined by Eq. (13) which is a function of temperature and results in temperature dependant buckling curves, which were found in [34] to be required for stainless steel columns in fire. Table 4 presents the proposed values for the β and η parameters, which were calibrated against the F.E. data for austenitic, duplex and ferritic SHS, RHS and CHS stainless steel columns generated in [34].

$$N_{b,fi,t,Rd} = \frac{\chi_{fi} A k_{y,\theta} f_y}{\gamma_{M,fi}} \quad (11)$$

$$\chi_{fi} = \frac{1}{\varphi_\theta + \sqrt{\varphi_\theta^2 - \beta\bar{\lambda}_\theta^2}} \leq 1.0 \text{ with } \varphi = 0.5\left[1 + \alpha\bar{\lambda}_\theta + \beta\bar{\lambda}_\theta^2\right] \quad (12)$$

$$\alpha = \eta \sqrt{\frac{235}{f_y}\frac{E}{210000}} \sqrt{\frac{k_{E,\theta}}{k_{y,\theta}}} \quad (13)$$

4.3 Combined loading interaction factors

4.3.1 Numerical modelling assumptions

A series of numerically derived interaction factors were produced using the validated numerical modelling approach presented in Section 3 which formed the basis for the calibration of the new proposed combined loading interaction factor formulae for design presented in 4.2.2. For the purpose of this numerical study, the beam-column members were modelled under isothermal loading conditions, where they were subjected to a given uniform temperature θ, incorporating the reduced stress-strain data corresponding to the modelled temperature θ, followed by applying a combined axial compressive load and uniform bending moment along the length of the members until failure. This approach, which has been also adopted in other similar numerical modelling investigations e.g. in [14,16,18-19,22], was deemed acceptable, since the F.E. models did not explicitly include the effect of time dependent factors such as creep. The parametric models covered beam-column members of RHS and CHS profiles subjected to varying levels of axial load to uniform bending moment ratios subjected to elevated temperatures of 200 °C, 400 °C, 600 °C and to 800 °C.

All the beam-column models were subjected to bending about one axis only. For the RHS models, both major and minor axis bending cases were modelled i.e. (1) combined axial load and major axis bending and (2) combined axial load and minor axis bending. Beam-columns of austenitic, duplex and ferritic stainless steel grades were modelled. For each stainless steel grade and elevated temperature considered, members with non-dimensional slenderness $\bar{\lambda}_\theta$ between 0.5 and 3.0 were modelled. Both modelled cross-sections were classified as fully effective, as there were found to give lower combined loading reduction factors. RHS had plate slenderness $\bar{\lambda}_p = 0.34, 0.36, 0.30$ and CHS had local slenderness $\bar{\lambda}_c = 0.18, 0.19, 0.16$ at room temperature for austenitic, duplex and ferritic grades, respectively. The cross-section slenderness values $\bar{\lambda}_p$ and $\bar{\lambda}_c$ were calculated using Eqs (14) and (15), respectively. In Eq. (14), $f_{cr,p}$ is the elastic critical buckling stress of the plate element, f_y is the yield stress, b and t are the larger flat plate width and thickness of the section, respectively, E is the Young's modulus, k_σ is the plate buckling coefficient, set to 4.0 for internal plate elements subjected to uniform compressive stress state and v stands for the Poisson's ratio taken as 0.3. In Eq. (15), $f_{cr,c}$ is the elastic critical buckling stress for a circular hollow section, D is the section outer diameter, and all other symbols are as previously defined. Table 5 presents a summary of the parametric models, where in total, 1134 RHS and 604 CHS parametric results were generated.

$$\bar{\lambda}_p = \sqrt{\frac{f_y}{f_{cr,p}}} = \left(\frac{b}{t}\right)\left(\frac{f_2}{E}\right)^{0.5}\left(\frac{12(1-\nu^2)}{\pi^2 k_\sigma}\right)^{0.5} \quad (14)$$

$$\bar{\lambda}_c = \sqrt{\frac{f_y}{f_{cr,c}}} = \left(\frac{f_2 D}{2tE}\right)^{0.5}\left(\sqrt{3(1-\nu^2)}\right)^{0.5} \quad (15)$$

The room temperature material properties were taken as those recommended in [30] for numerical parametric studies of stainless steel structures. The elevated temperature two-stage Ramberg-Osgood material model recommended in [11] was used to describe the elevated temperature stress-strain behaviour. The elevated temperature strength and stiffness reduction factors were obtained from [11] as those specified for Austenitic I, Duplex II and Ferritic II groups. The beam-columns had pin-ended boundary conditions about the axis of buckling which was the same as the axis of the applied bending moment. For major axis (y-y) flexural buckling and major axis applied bending moment the displacement (u) and rotational (ur) boundary conditions were u_x = free, u_y = u_z = fixed and ur_x = ur_z = fixed and ur_y = free at the loaded end and u_x = u_y = u_z = fixed and ur_x = ur_z = fixed and ur_y = free at the other end. For minor axis (z-z) flexural buckling and minor axis applied bending moment the displacement (u) and rotational (ur) boundary conditions were u_x = free, u_y = u_z = fixed and ur_y = ur_z = fixed and ur_z = free at the loaded end and u_x = u_y = u_z = fixed and ur_x = ur_y = fixed and ur_z = free at the other end. The initial global geometric imperfections amplitude was set equal to the EN 1090-2 [35] specified tolerance limit equal to $L/1000$, where L is the member length. The initial local geometric imperfection amplitude was set to $b/200$, where b is the section width, for the RHS members and $0.008D$, where D is the diameter, for the CHS members as recommended in EN 1993-1-5-Annex C [36].

The loading was applied in two steps, firstly, a concentric compressive axial load was applied to the beam-column members, which was maintained constant, followed by an increasing equal uniaxial bending moment at the member ends until failure. The applied axial compressive load $N_{Ed,\theta}$ was taken as a portion of the member elevated temperature flexural buckling resistance $N_{b,y,Rd,fi}$ or $N_{b,z,Rd,fi}$ i.e. $N_{Ed,\theta} = n\, N_{b,y,Rd,fi}$ or $n\, N_{b,z,Rd,fi}$ with n (load level) values equal to 0.3, 0.4, 0.5, 0.6, and 0.7 and $N_{b,y,Rd,fi}$ and $N_{b,z,Rd,fi}$ capcities obtained from the proposed flexural buckling curves in [34]. Hence, a range of axial load to bending moment ratios were considered. The load-deformation response was obtained by using a modified Riks analysis method in Abaqus.

4.3.2 Calibration of interaction factor formulae

Numerically derived interaction factors, k_y and k_z, were obtained by rearranging Eqs (9) and (10), as presented by Eqs (16) and (17), respectively where $N_{fi,Ed}$, $M_{y,fi,Ed}$ and $M_{z,fi,Ed}$ were set to the F.E. obtained values, $N_{b,y,Rd,fi}$ and $N_{b,z,Rd,fi}$ were set to the elevated temperature flexural buckling resistances obtained from the proposed method in [34] and $M_{c,y,Rd,fi}$ and $M_{c,z,Rd,fi}$ are the elevated temperature cross-section resistances determined according to EN 1993-1-2 [9] design provisions. All partial factors of safety were set to unity.

$$k_y = \left(1 - \frac{N_{fi,Ed}}{N_{b,y,Rd,fi}}\right) \Big/ \left(\frac{M_{y,fi,Ed}}{M_{c,y,Rd,fi}}\right) \tag{16}$$

$$k_z = \left(1 - \frac{N_{fi,Ed}}{N_{b,z,Rd,fi}}\right) \Big/ \left(\frac{M_{z,fi,Ed}}{M_{c,z,Rd,fi}}\right) \tag{17}$$

Examples of the derived interaction factors for RHS and CHS austenitic, duplex and ferritic beam-column members subjected to 200 °C temperature and with load level n = 0.2 are presented in Figure 8. Figure 8 demonstrates the relationship between the derived interaction factors k and the non-dimensional slenderness $\bar{\lambda}_\theta$. It can be observed that the relationship between the non-dimensional member slenderness $\bar{\lambda}_\theta$ and interaction factors k has a steep slope in the low member slenderness range but a relatively steady slope in the high member slenderness range.

A bi-linear equation can therefore be employed for the k parameter in the beam-column design equations. Eq. (18) presents the expression adopted by Greiner and Linder [37] and Boissonnade et al. [38] for carbon steel beam-column members and, more recently, for stainless steel tubular members at room temperature by Zhao et al. [39]. The coefficients D_1 and D_2 describe the linear part of the relationship between the member slenderness $\bar{\lambda}_\theta$ and the interaction factor k over the low slenderness range i.e. when $\bar{\lambda}_\theta$ falls below the limiting value D_3. At $\bar{\lambda}_\theta$ values beyond D_3, the interaction factor k remains constant equal to $1+D_1(D_3-D_2)n$. For each load level, a regression fit of Eq. (18) through the corresponding numerical dataset, over a member slenderness range of 0.2 and 1.2, was made to determine the values of the D_1 and D_2 coefficients. The D_1 and D_2 values were then averaged for all the load levels (i.e. $0.2 \leq n \leq 0.7$) for each specified temperature θ. Then, the values of D_3 were calculated based on the fit of Eq. (13) to the upper bound of the assembled numerical dataset for low axial compressive load level (i.e. $n \leq 0.4$). Table 6 reports the values of D_1, D_2 and D_3 for each of the material grades and temperatures considered. A set of D_1, D_2 and D_3 values for all temperatures in the range of 200-800°C, based on the average of the temperature specific values, is also proposed in Table 6. Figure 9 presents the F.E. derived and

the proposed interaction factors for the RHS 150×100×14 (major axis), RHS 150×100×14 (minor axis) and for CHS 100×8 beam-columns at 200 °C. In Figure 9, there is a large difference between the proposed combined loading interaction factors and the F.E. derived values at high slenderness and at high load levels. This difference was also observed in similar previous derivation of beam-column interaction factors [39]. However, since for beam-column members with high slenderness and high axial load levels the response is governed by flexural buckling, the contribution of the bending resistance term is relatively small, and the effect of this error on the overall predicted resistance are negligible.

$$k = 1 + D_1\left(\bar{\lambda}_\theta - D_2\right)n, \text{ but } k \le 1 + D_1(D_3 - D_2)n \quad (18)$$

5. Comparison of predicted resistances with proposed and codified methods

5.1 FE parametric data

The accuracy and the reliability of the proposed design approach was assessed through a comparison against a large number of F.E. results, which were generated through parametric study. In the parametric study, beam-column performance data for RHS and CHS stainless steel members were generated. For the modelled RHS, the outer depth and width of the cross-section were set equal to 200 mm and 100 mm, respectively, giving to a cross-section aspect ratio of 2.0. For the CHS, the outer diameter was set 100 mm. The cross-section thicknesses, 15 mm and 6 mm for RHS and 6 mm and 1.5 mm for CHS, were selected to ensure fully effective and slender cross-sections. The cross-section slenderness for the austenitic, duplex and ferritic models were $\bar{\lambda}_p$ = 0.42, 0.44, 0.37 (fully effective) and $\bar{\lambda}_p$ = 1.01, 1.07, 0.90 (slender) for RHS and $\bar{\lambda}_c$ = 0.20, 0.22, 0.19 (fully effective) and $\bar{\lambda}_c$ = 0.41, 0.44, 0.38 (slender) for CHS, respectively. The lengths of the beam-column members were varied to cover a wide spectrum of member slendernesses between 0.2 and 2.0. The axial compressive load was applied concentrically and ranged from load levels of n = 0 to 1, increasing in steps of 0.1, followed by applying a moment concentrically. This allowed a broad range of axial load to bending moment ratios to be considered. In total, 3180 parametric study results were generated, including 1980 for the RHS (major and minor axes) and 1260 for CHS.

5.2 Analysis of results and reliability analysis

The numerical results generated were compared with the strength predictions from the European EN 1993-1-2 [9] and the proposed approaches. The predicted failure load $N_{u,pred,\theta}$ was determined assuming proportional loading, as defined in Figure 10 and also adopted in [39], where the axial load ratio $N_\theta/N_{.R.,\theta}$ is plotted against the bending moment ratio $M_\theta/M_{.R.,\theta}$. In Figures 10, N_θ and M_θ

are the F.E. ($N_{u,\,F.E.,\theta}$ and $M_{u,\,F.E.,\theta}$) or predicted ($N_{u,pred,\theta}$ and $M_{u,pred,\theta}$) axial compressive load and bending moment capacities of the beam-column members under consideration, while $N_{.R.,\theta}$ and $M_{.R.,\theta}$ are their corresponding flexural buckling load, under pure axial load, and bending moment, under pure bending moment, resistances, respectively at elevated temperature. A $N_{u,\,F.E.,\theta}/N_{R,\theta}$ ratio of value greater than unity indicates that the F.E. data point lies on the safe side of the design interaction curve. Figures 11 and 12 show the comparison results for the EN 1993-1-2 [9] design rules and the proposed design method, respectively, where the F.E. to predicted failure load ratio $N_{u,\,F.E.,\theta}/N_{u,pred,\theta}$ is plotted against the angle parameter φ for RHS and CHS members. The angle parameter φ was determined as defined by Eq. (19) and shown in Figure 10, where $\varphi = 0°$ and $\varphi = 90°$ correspond to pure bending and pure compression cases, respectively. The measured geometric and material properties were used in all the comparisons and all partial safety factors have been set equal to unity. Table 7 reports the mean and COV values for the FE-to-predicted failure load ratios for the austenitic, duplex and ferritic stainless steel beam-columns. For each stainless steel grade, comparisons are made between the EN 1993-1-2 [9] and the proposed methods and the F.E. beam-column resistances. The comparisons shown in Figure 11 and Table 8 show that the current EN 1993-1-2 [9] method gives inaccurate and scattered strength predictions. In comparison, it is shown in Figure 12 and Table 8 that significantly higher degrees of accuracy and consistency are obtained from the proposed design approach for stainless steel tubular beam-column members for all the considered loading combinations. Figure 13 provides a comparison between EN 1993-1-2 $N_{u,pred,\theta}$ and proposed $N_{u,pred,\theta}$ for austenitic, duplex, and ferritic stainless steel beam-columns.

$$\varphi = \tan^{-1}\left[\frac{N_{u,F.E.,\theta}/N_{R,\theta}}{M_{u,F.E.,\theta}/M_{R,\theta}}\right] \tag{19}$$

The reliability of the proposed design approach was assessed through statistical analyses and results were compared with those for the EN 1993-1-2 design rules. The reliability assessment procedures outlined by Kruppa et al. [40] for the verification of fire design rules were employed herein. The reliability criteria involves three requirements, which include:

- Criteria (1) - the percentage amount of the predicted resistances on the unsafe side by more than 15% of the actual resistances to be zero
- Criteria (2) - the percentage of the predicted resistance on the unsafe side to be less than 20%

- Criteria (3) - the mean percentage difference between the predicted and actual resistances be on the safe side and less than zero.

A summary of the safety assessment results is presented in Table 8. It is shown that the proposed design method meets all the reliability criteria. In contrast, EN 1993-1-2 fails to comply with the reliability criteria for all considered cases, except for the CHS ferritic stainless steel beam-column members.

6. Conclusion

This paper provides a thorough analysis of the elevated temperature response of stainless steel rectangular and circular hollow sections beam-column members through a numerical modelling investigation. Numerical models of stainless steel beam-columns were developed and validated against a selection of room and elevated temperature beam-columns tests reported in the literature. The validated models were subsequently used to perform parametric studies and to generate a pool of structural performance data. The numerical data were adopted to evaluate the level of accuracy of the existing structural fire design provision in EN 1993-1-2. The findings indicated that the current European fire design provisions led to inaccurate design strength predictions, giving unsafe results with a high degree of scatter, in all cases considered, apart from for the CHS ferritic stainless steel members. New design recommendations were therefore proposed and statistically verified. This included proposing a new elevated temperature flexural buckling formulation for SHS, RHS and CHS stainless steel columns to obtain accurate predictions of the pure compression capacity and also new combined loading interaction factors for the combined axial load and bending moment interaction equations. The proposed modifications were shown to offer significantly more accurate and consistent capacity predictions.

References

[1] EN 1993-1-4. Eurocode 3: Design of Steel Structures – Part 1–4: General Rules – Supplementary Rules for Stainless Steels. European Committee for Standardization, Brussels (2015).

[2] AS/NZS 4673. Cold-formed Stainless Steel Structures. Australian/New Zealand Standard, Sydney (2001).

[3] AISC Design Guide 27: Structural Stainless Steel. American Institute of Steel Construction (2013).

[4] SEI/ASCE-8. Specification for the Design of Cold-formed Stainless Steel Structural Members American Society of Civil Engineers, Reston (2002).

[5] CECS-410. Technical Specification for Stainless Steel Structures. China Planning Press, Beijing (in Chinese) (2015).

[6] J. Chen, B. Young. Stress-strain curves for stainless steel at elevated temperatures.

[7] E. Mirambell, E. Real. On the calculation of defections in structural stainless steel beams: an experimental and numerical investigation. Journal of Constructional Steel Research, 54(1), (2000), 109-133.

[8] L. Gardner, A. Insausti, K.T. Ng, M. Ashraf. Elevated temperature material properties of stainless steel alloys. Journal of Constructional Steel Research, 66 (5) (2010), pp. 634-647

[9] EN 1993-1-2 Eurocode 3: Design of Steel Structures – Part 1–2: General rules - Structural fire design. European Committee for Standardization, Brussels (2005).

[10] Y. Huang, B. Young. Stress-strain relationship of cold-formed lean duplex stainless steel at elevated temperatures. Journal of Constructional Steel Research, 92 (2017), pp. 103-113.

[11] Stainless Steel Design Manual (fourth edition), Steel Construction Institute (SCI) (2017).

[12] K.T. Ng, L. Gardner. Buckling of stainless steel columns and beams in fire. Engineering Structures. 29 (5) (2007), pp. 717-730.

[13] S. Fan, X. Ding, W. Sun, L. Zhang, M. Liu. Experimental investigation on fire resistance of stainless steel columns with square hollow section. Thin-Walled Structures, 98 (2016), pp. 196-211

[14] Y. Huang, B. Young. Finite element analysis of cold-formed lean duplex stainless steel columns at elevated temperatures. Thin-Walled Structures, 143 (2019), 106203

[15] N. Tondini, B. Rossi, J.M. Franssen. Experimental investigation on ferritic stainless steel columns in fire. Fire Safety Journal, 62 (2013), pp. 238-248.

[16] N. Lopes, P. Vila Real, L.S. Silva, J.M. Franssen. Axially loaded stainless steel columns in case of fire. Journal of Structural Fire Engineering, 1(1), (2010), 43-59.

[17] F. Arrais, N. Lopes, P. Vila Real. Numerical study of fire resistance of stainless steel circular hollow section columns. Journal of Fire Sciences, 38(2) (2020), pp. 156-172

[18] Y. Huang, B. Young. Structural performance of cold-formed lean duplex stainless steel beams at elevated temperatures. Thin-Walled Structures, 129, (2018), pp. 20-27.

[19] M. Kucukler, Z. Xing, L. Gardner. Behaviour and design of stainless steel I-section columns in fire. Journal of Constructional Steel Research. 165, (2020), 105890

[20] Z. Xing, O. Zhao, M. Kucukler, L. Gardner. Fire testing of austenitic stainless steel I-section beam–columns. Thin-Walled Structures, 164, (2022), 107916

[21] Y. Huang, J. Chen, Y. He, B. Young. Design of cold-formed stainless steel RHS and SHS beam-columns at elevated temperatures. Thin-Walled Structures, 165, (2021), 107960

[22] G. Segura, A. Pournaghshband, S. Afshan, E Mirambell. Numerical simulation and analysis of stainless steel frames at high temperature. Engineering Structures, 227, (2021), 111446

[23] A. Pournaghshband, S. Afshan, A.S.J. Foster. Structural fire performance of axially and rotationally restrained stainless steel columns. Thin Walled Structures, 137, (2019), 561–572

[24] A. Pournaghshband, S. Afshan, M. Theofanous. Elevated temperature performance of restrained stainless steel beams. Structures, 22, (2019), 278-290

[25] O. Zhao, L. Gardner, B. Young. Buckling of ferritic stainless steel members under combined axial compression and bending. Journal of Constructional Steel Research, 117 (2016), pp. 35-48.

[26] O. Zhao, L. Gardner, B. Young. Testing and numerical modelling of austenitic stainless steel CHS beam-columns. Engineering Structures, 111 (2016), pp. 263-274.

[27] J. Pauli, D. Somaini, M. Knobloch, M. Fontana. Experiments on steel columns under fire conditions. Report. Swiss Federal Institute of Technology Zurich, Institute of Structural Engineering (2012).

[28] ABAQUS. Version 2016, Dassault Systmes Simulia Corp. USA 2016.

[29] S. Fan, X. Ding, W. Sun, L. Zhang, M. Liu. Numerical investigation on fire resistance of stainless steel columns with square hollow section under axial compression. 98, (2016), pp. 185-195.

[30] S. Afshan, O. Zhao, L. Gardner. Standardised material properties for numerical parametric studies of stainless steel structures and buckling curves for tubular columns. Journal of Constructional Steel Research, 152 (2019), pp. 2-11.

[31] L. Gardner, D.A. Nethercot. Numerical modelling of stainless steel structural components – a consistent approach. Journal of Structural Engineering (ASCE), 130 (10) (2004), pp. 1586-1061.

[32] R.B. Cruise, L. Gardner. Residual stress analysis of structural stainless steel sections. Journal of Constructional Steel Research. 64, (2008), pp. 352-366.

[33] Cruise R.B., Gardner L. Strength enhancements induced during cold forming of stainless steel sections. Journal of Constructional Steel Research, (2008);64(11):1310–6.

[34] A. Mohammed, S. Afshan. Numerical modelling and fire design of stainless steel hollow section columns. Thin-Walled Structures, 144 (2019), pp. 1-13 [106243].

[35] EN 1090-2. 2008. Execution of steel structures and aluminium structures - Part 2: Technical requirements for steel structures. Brussels: European Committee for Standardization.

[36] EN 1993-1-5. Eurocode 3 - Design of steel structures - Part 1-5: Plated structural elements. Brussels: European Committee for Standardization, Brussels (2006).

[37] R. Greiner, J. Lindner. Interaction formulae for members subjected to bending and axial compression in EUROCODE 3 – the Method 2 approach. Journal of Constructional Steel Research, 62(8) (2006), pp. 757–770.

[38] N. Boissonnade, J.P. Jaspart, J.P. Muzeau, M. Villette, M. New interaction formulae for beam-columns in Eurocode 3: The French–Belgian approach. Journal of Constructional Steel Research, 60 (2004), pp. 421-431.

[39] O. Zhao, L. Gardner, B. Young. Behaviour and design of stainless steel SHS and RHS beam-columns. Journal of Constructional Steel Research, 106, (2016) pp. 330-345.

[40] J. Kruppa. Eurocodes Fire parts: Proposal for a methodology to check the accuracy of assessment methods. CEN TC 250, Horizontal Group Fire, Document no: 99/130 (1999).

Figures

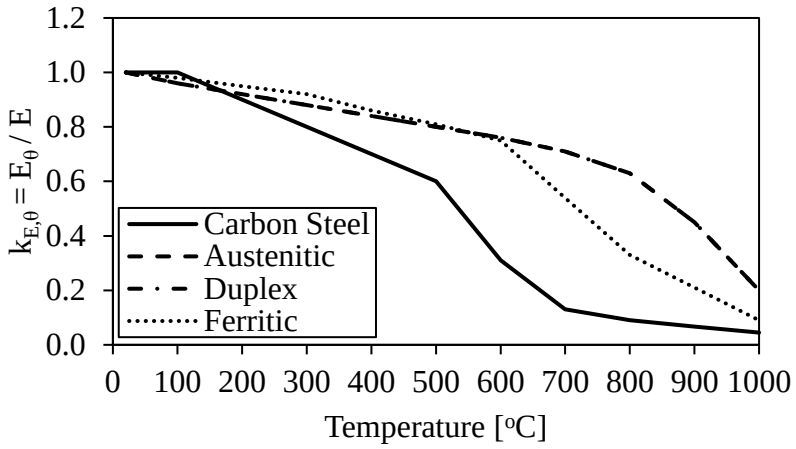

(a)

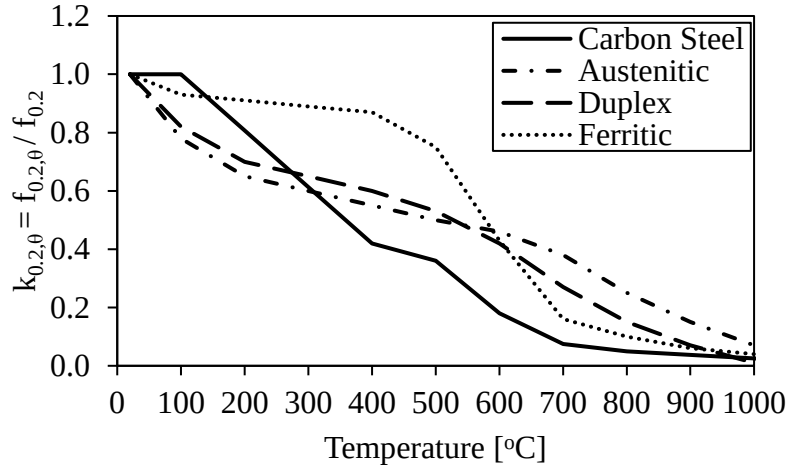

(b)

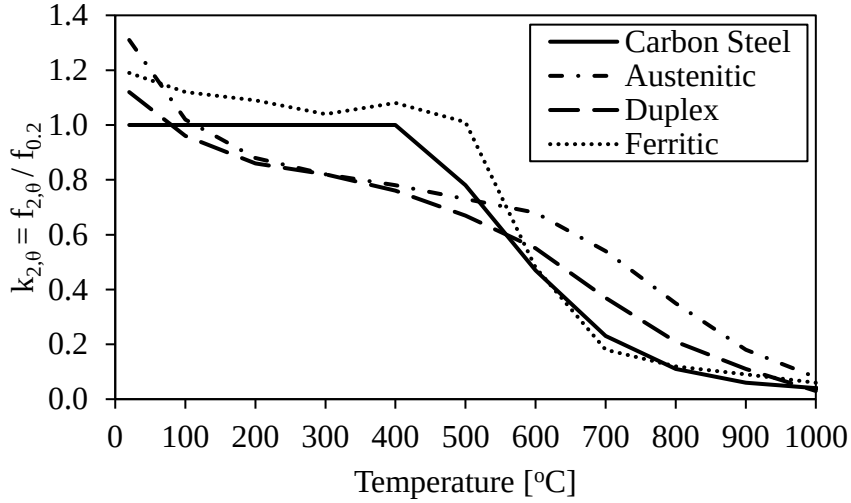

(c)

Figure 1: Influence of elevated temperature on the material properties of stainless steel and carbon steel in terms of reduction factors for (a) Youngs modulus, (b) 0.2% proof strength and (c) strength at 2% total strain (data are from [11] for stainless steel and [9] for carbon steel).

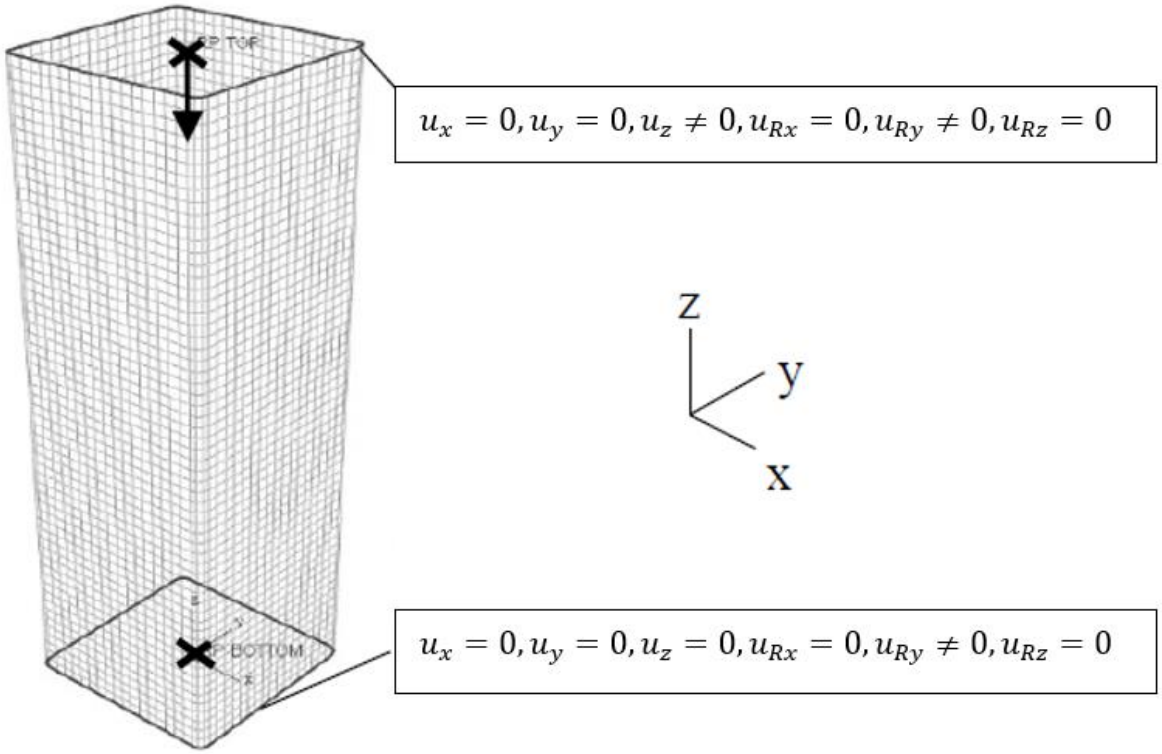

Figure 2: Boundary conditions for numerical model for buckling about major axis.

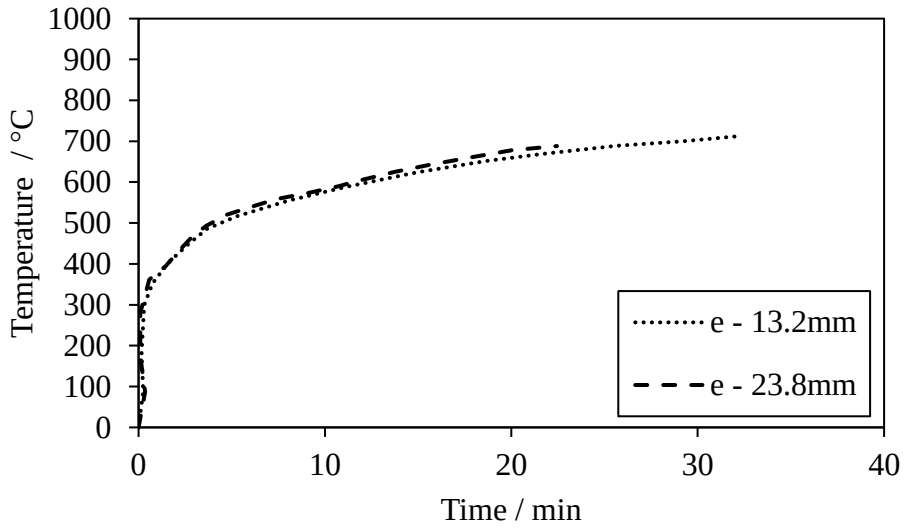

Figure 3: Comparison of test temperature development for SHS with eccentricity of 13.2mm and 23.8mm [13]

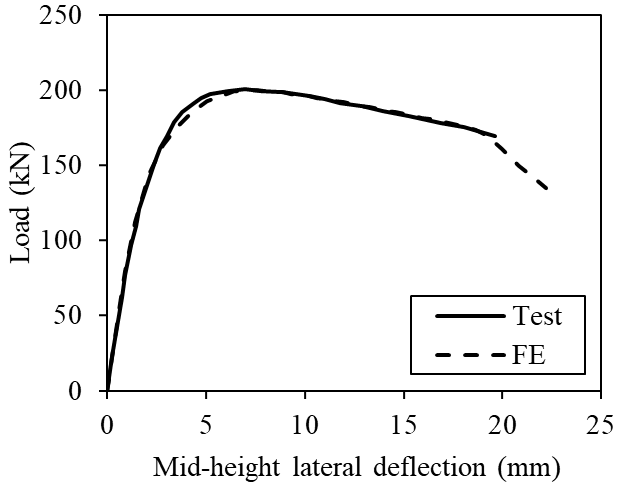

(a) SHS 60×60×3, e_y = 10 mm.

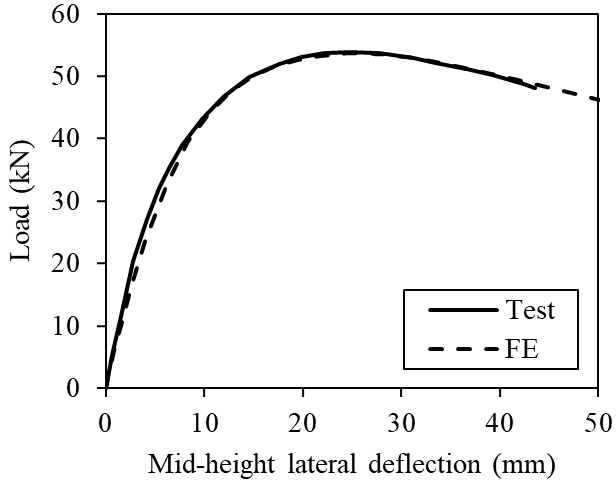

(b) CHS 60.5×2.8, e_y = 15 mm.

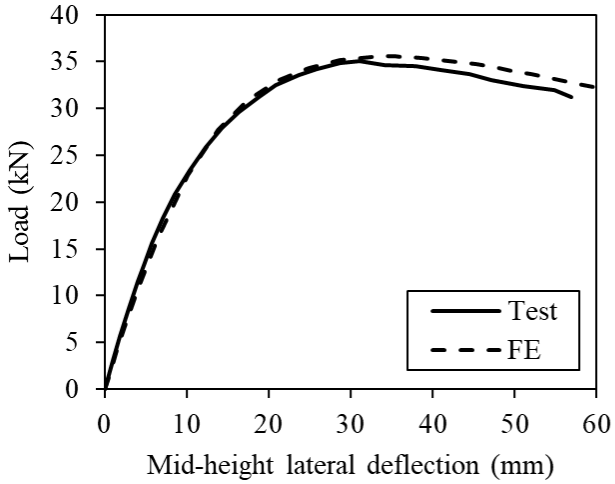

(c) CHS 60.5×2.8, e_y = 40 mm.

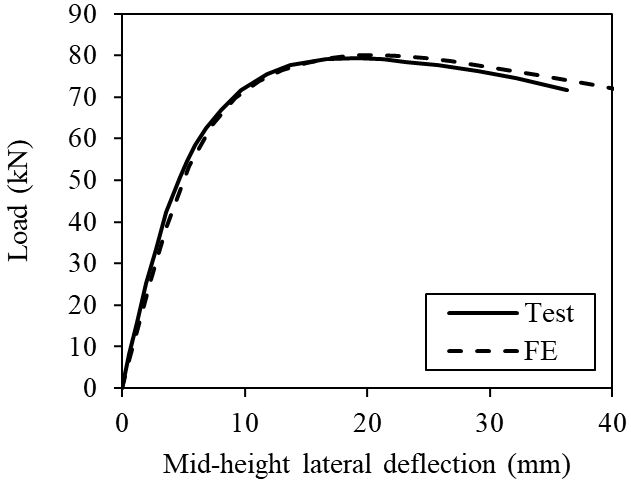

(d) CHS 76.3×3, e_y = 20 mm.

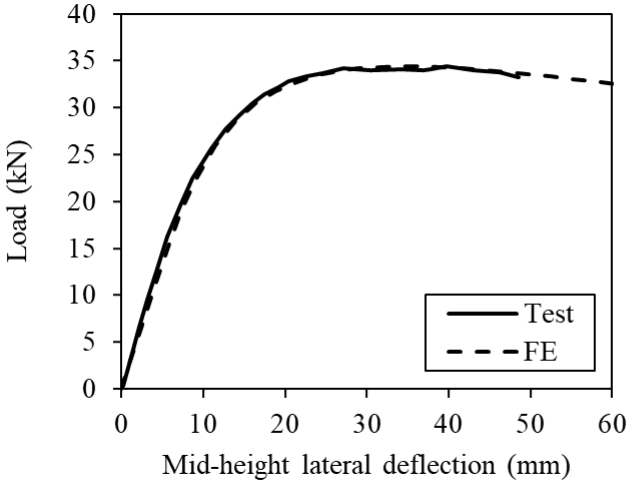

(e) CHS 76.3×3, e_y = 95 mm.

Figure 4: Test and FE load vs mid-height lateral deflection curves for the room temperature beam-column members.

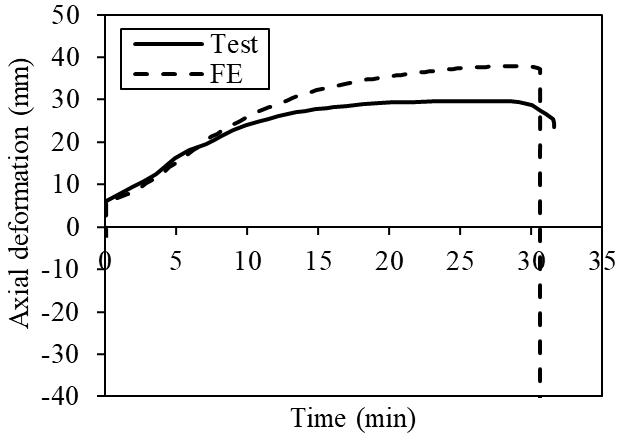

Figure 5: Test and FE axial displacement vs time for anisothermal beam-column member SHS 120×120×4 – e_y = 13.2 mm.

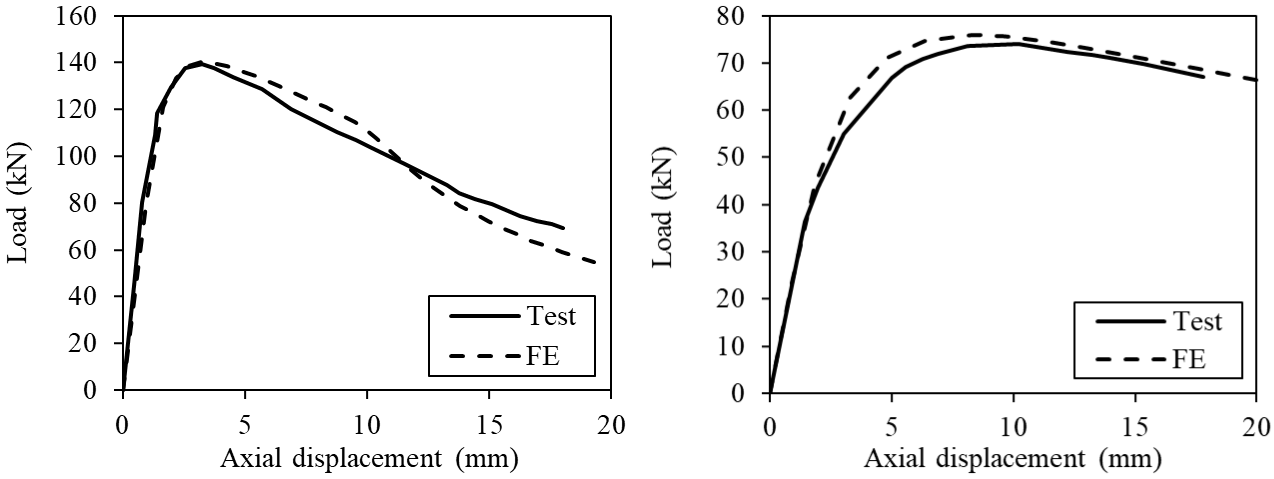

(a) e_z = 10 mm, θ = 400ºC

(b) e_z = 50 mm, θ = 400ºC

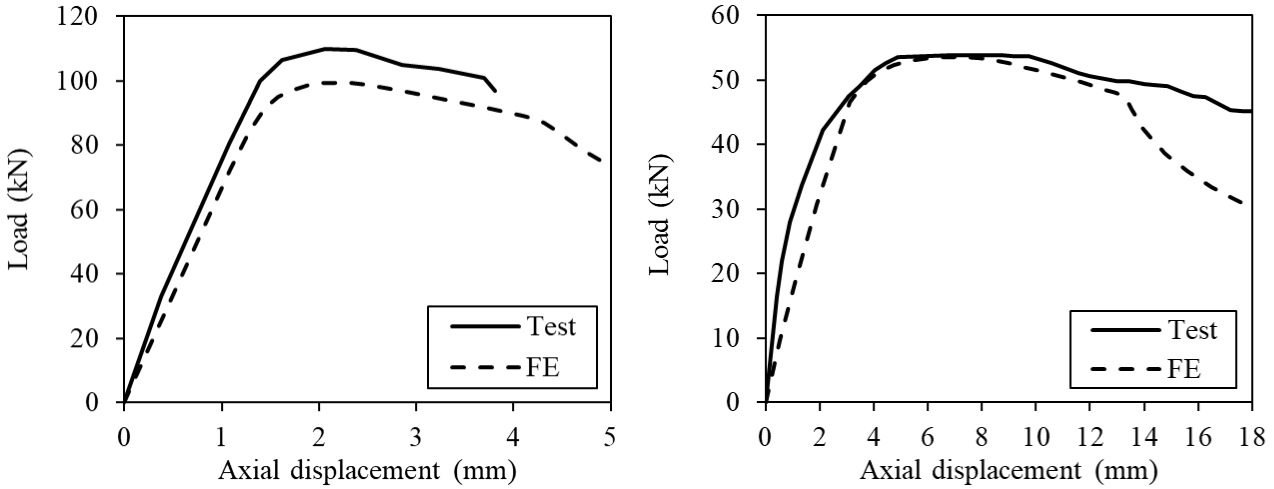

(c) e_z = 10 mm, θ = 550ºC

(d) e_z = 50 mm, θ = 550ºC

Figure 6: Test and FE load vs axial displacement curves for isothermal beam-column members.

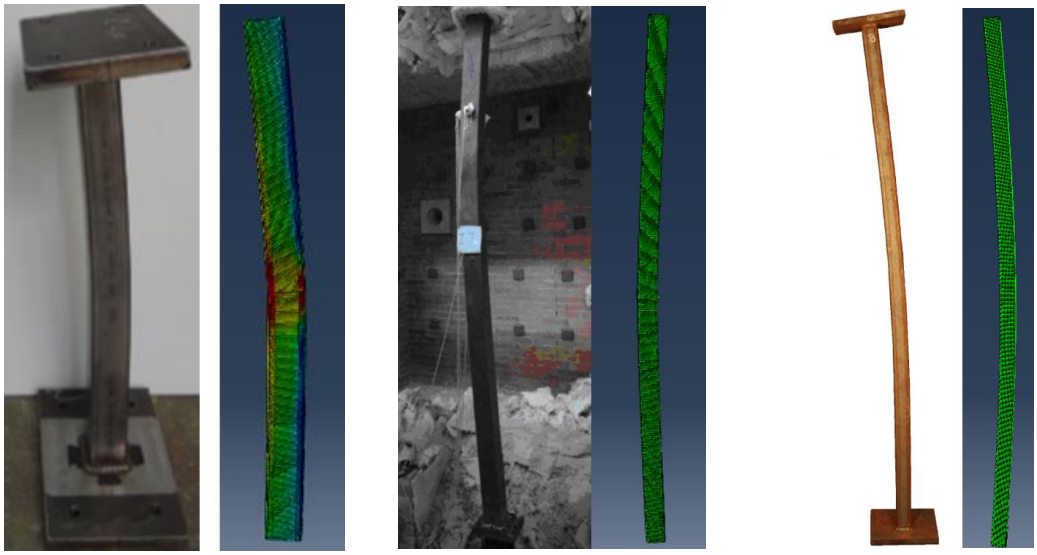

(a) SHS 60×60×3 e_z = 10 mm [25] (b) SHS 120×120×4 e_y = 13.2 mm [13] (c) RHS 120×60×3.6 e_z = 50mm, θ = 400°C [27]

Figure 7: Comparison of typical test and FE failure modes.

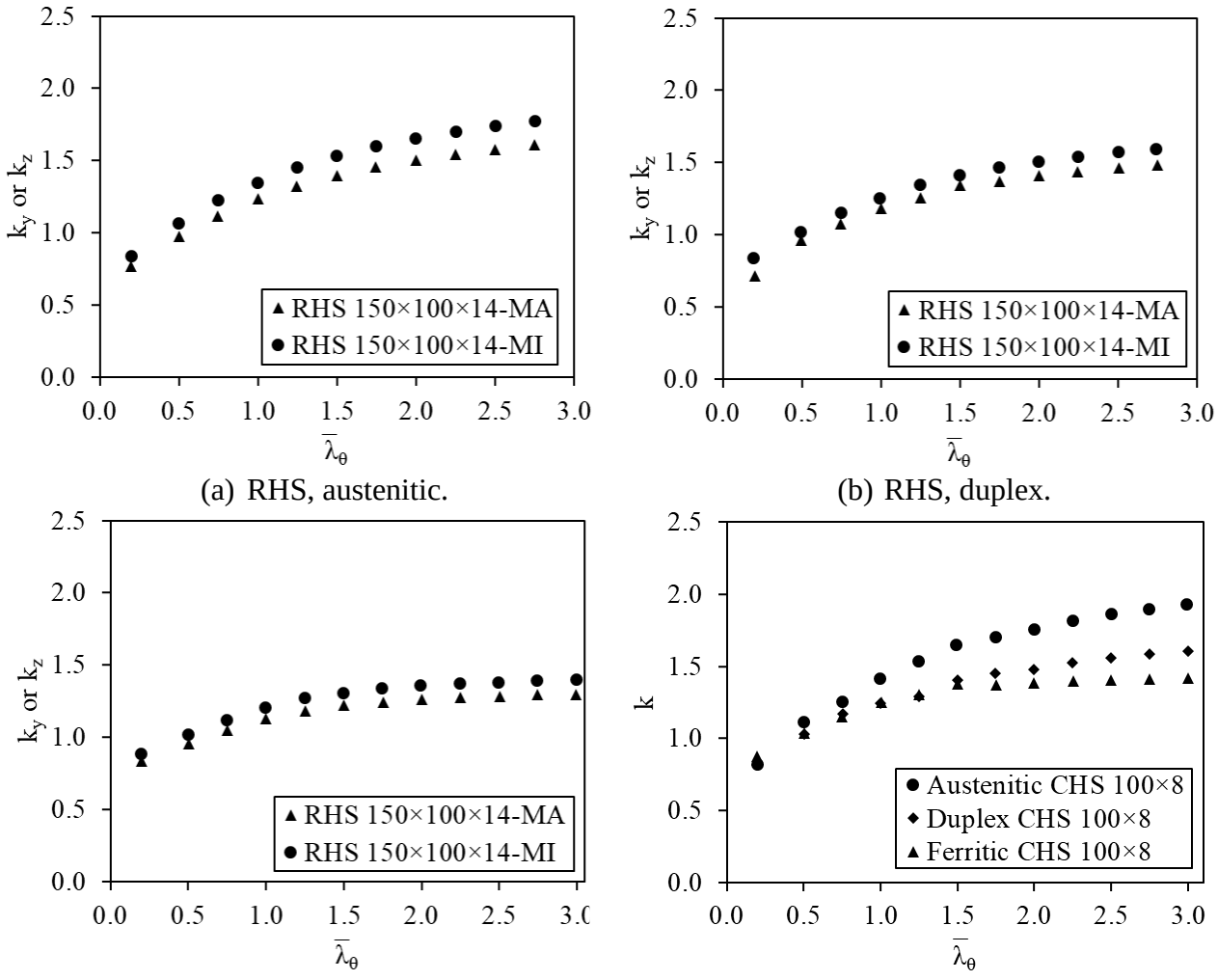

(a) RHS, austenitic. (b) RHS, duplex.

(c) RHS, ferritic. (d) CHS, Austenitic, duplex and ferritic

Figure 8: Examples of numerically derived k factors for RHS and CHS beam-columns.

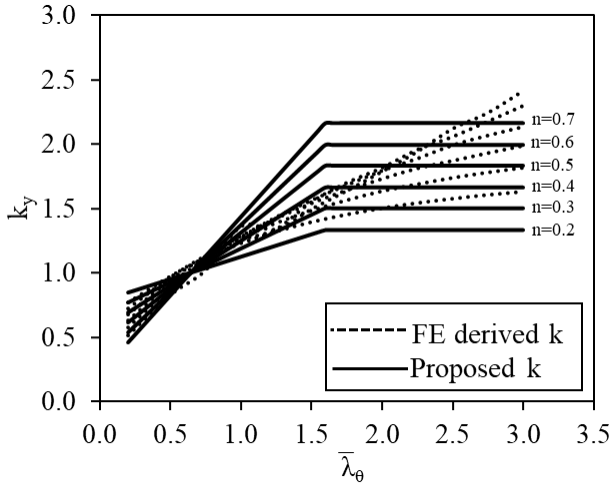

(a) RHS, austenitic, major axis.

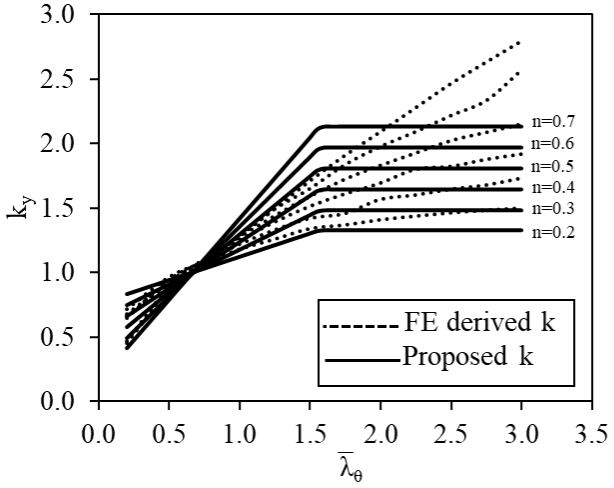

(b) RHS, duplex, major axis.

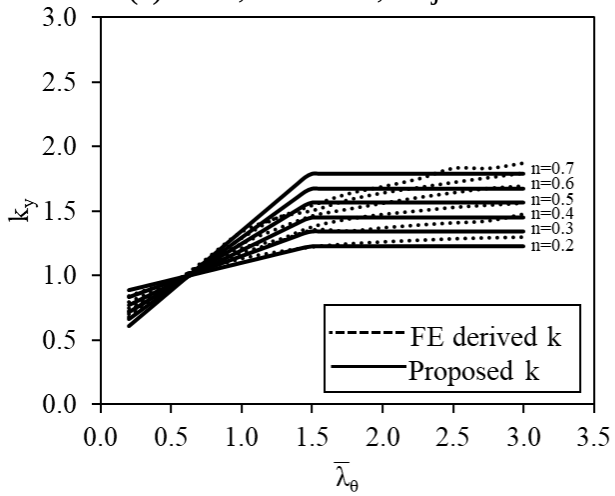

(c) RHS, ferritic, major axis.

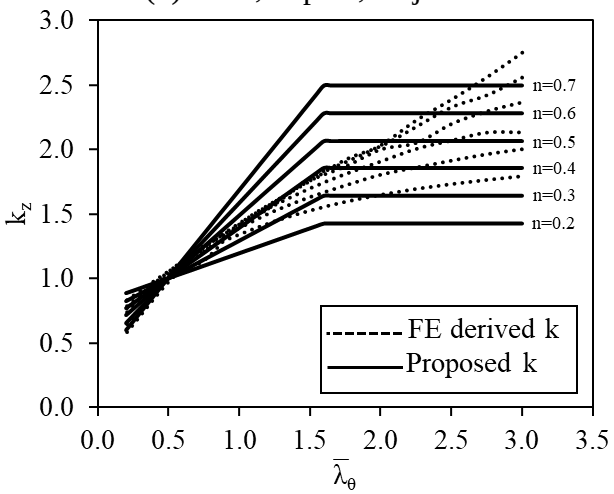

(d) RHS, austenitic, minor axis.

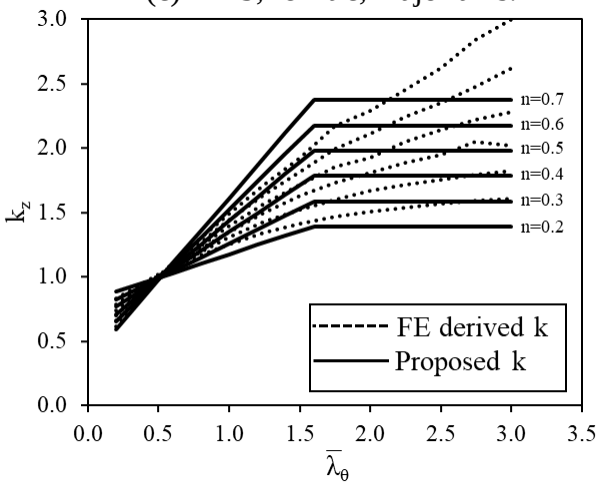

(e) RHS, duplex, minor axis.

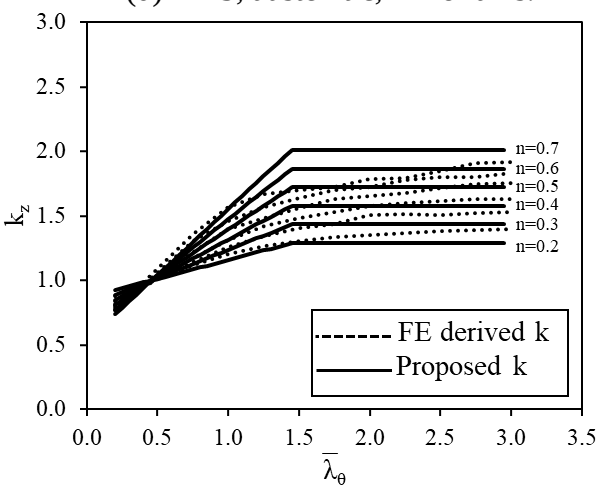

(f) RHS, ferritic, major axis.

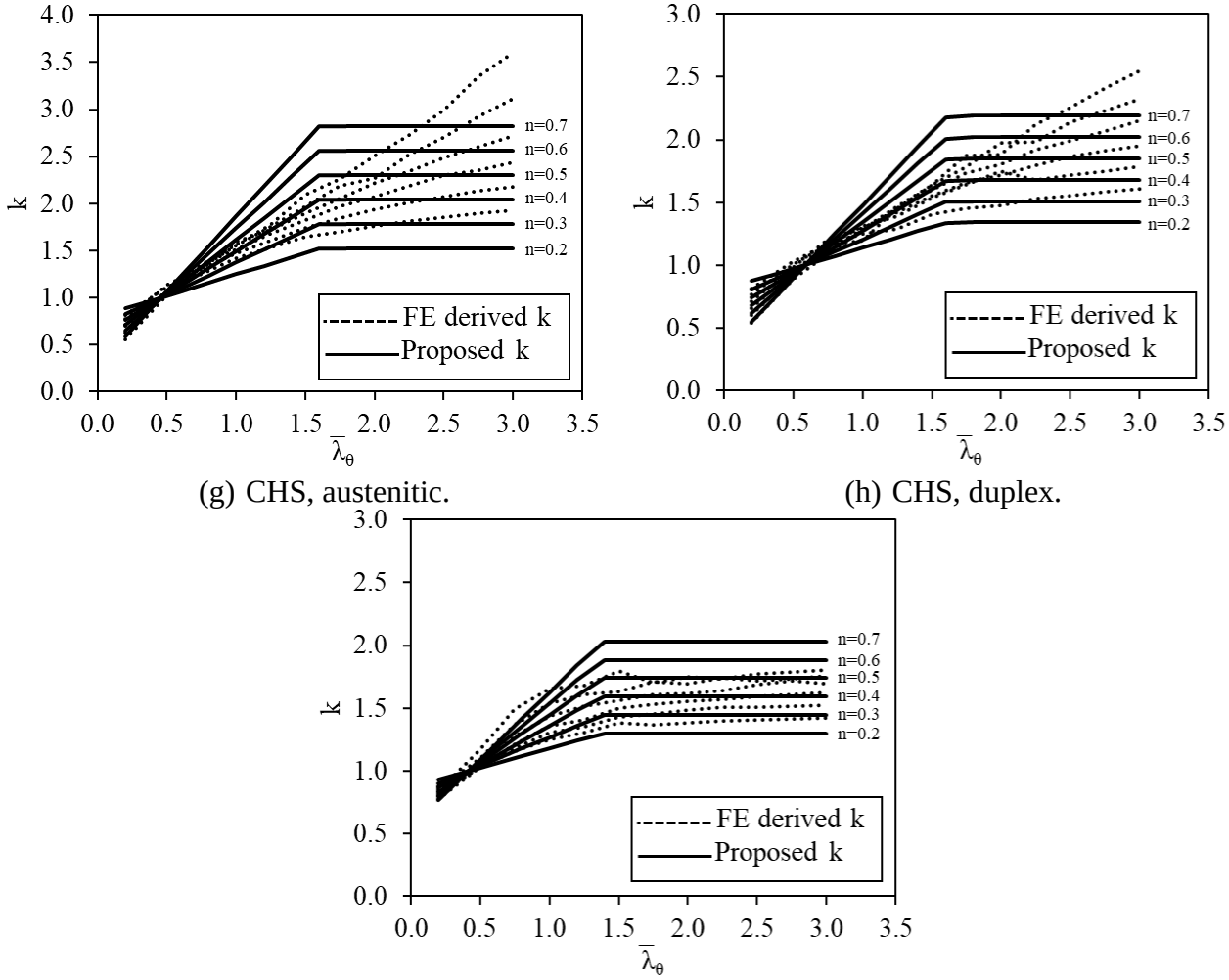

(g) CHS, austenitic. (h) CHS, duplex.

(i) CHS, ferritic.

Figure 9: Comparison between FE and proposed k factors for RHS and CHS members at θ = 200°C.

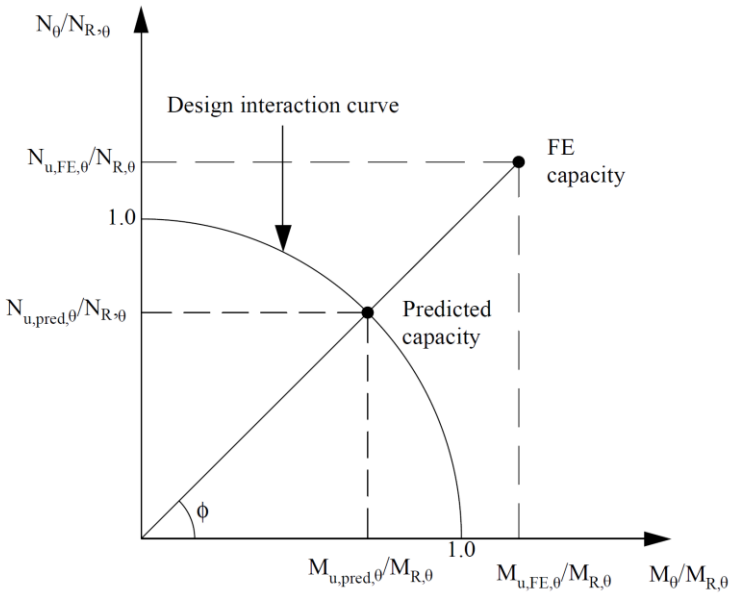

Figure 10: Axial load and moment interaction diagram and definition of symbols.

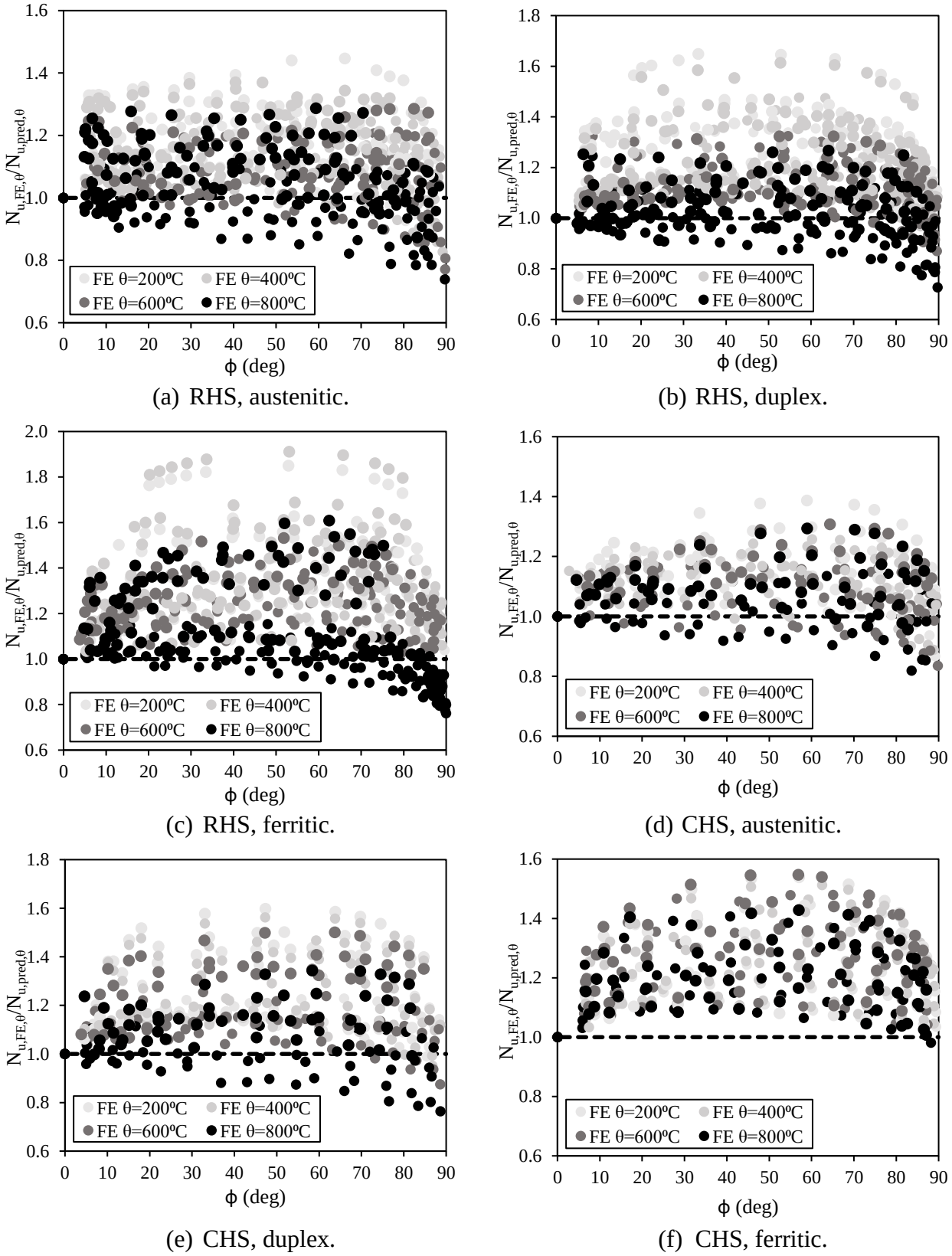

(a) RHS, austenitic. (b) RHS, duplex.

(c) RHS, ferritic. (d) CHS, austenitic.

(e) CHS, duplex. (f) CHS, ferritic.

Figure 11: Comparison of FE results $N_{u,FE,\theta}$ with EN 1993-1-2 [9] predicted resistances $N_{u,pred,\theta}$ for RHS and CHS beam-column members.

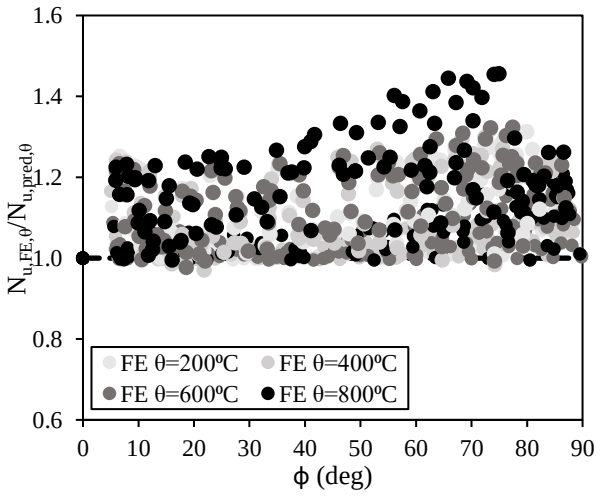

(a) RHS, austenitic.

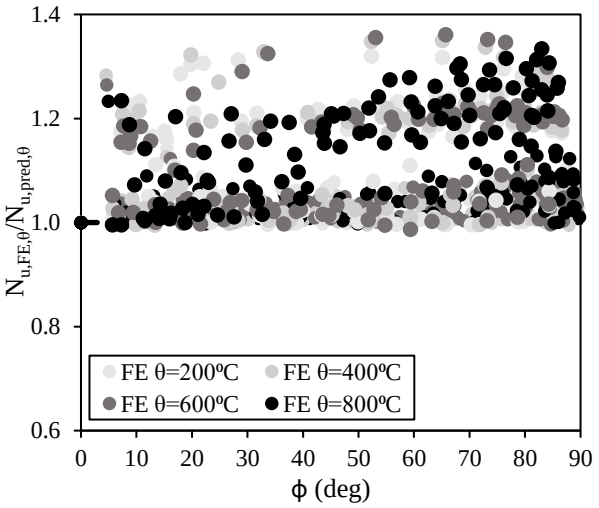

(b) RHS, duplex.

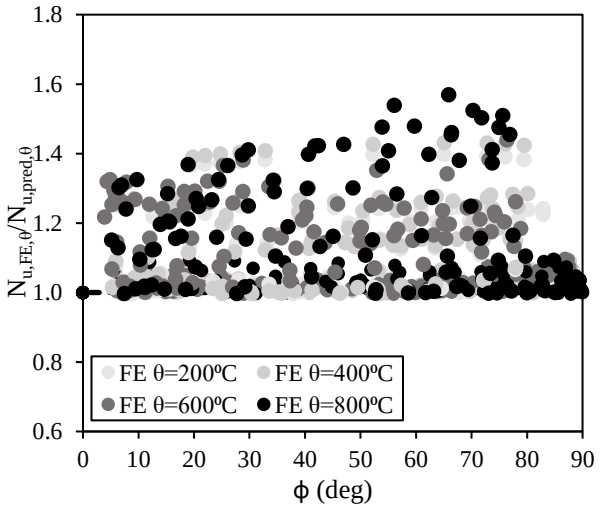

(c) RHS, ferritic.

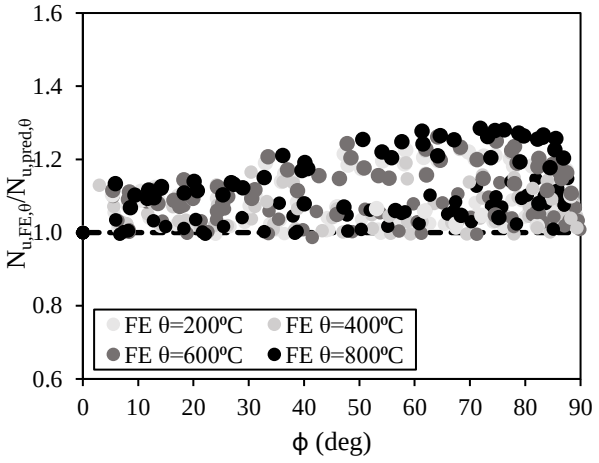

(d) CHS, austenitic.

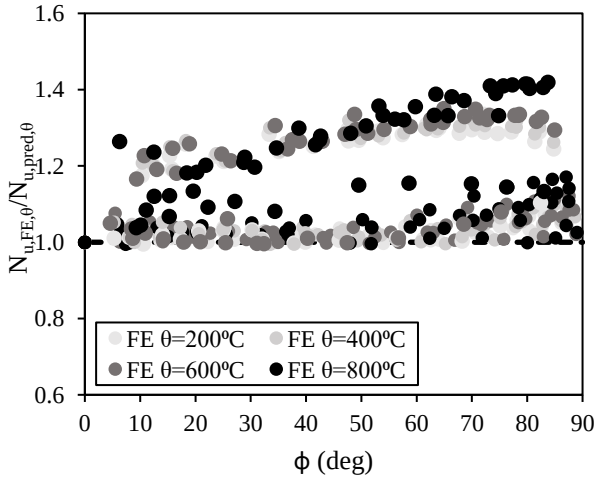

(e) CHS, duplex.

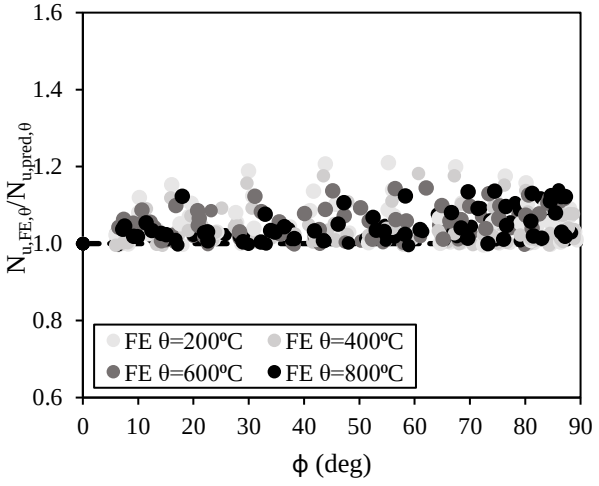

(f) CHS, ferritic.

Figure 12: Comparison of FE results $N_{u,FE,\theta}$ with the proposed method predicted resistances $N_{u,pred,\theta}$ for RHS and CHS beam-column members at θ

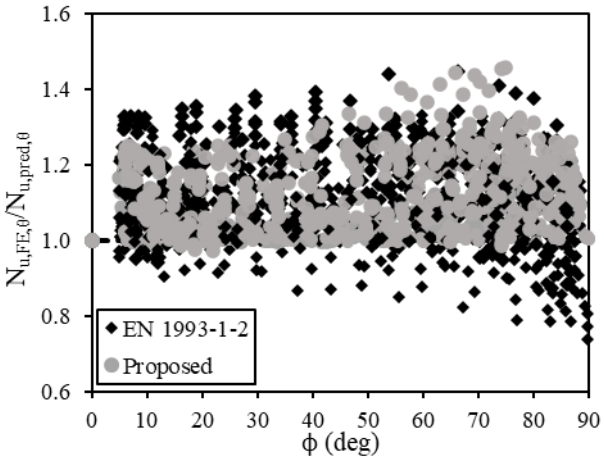

(a) RHS Austenitic

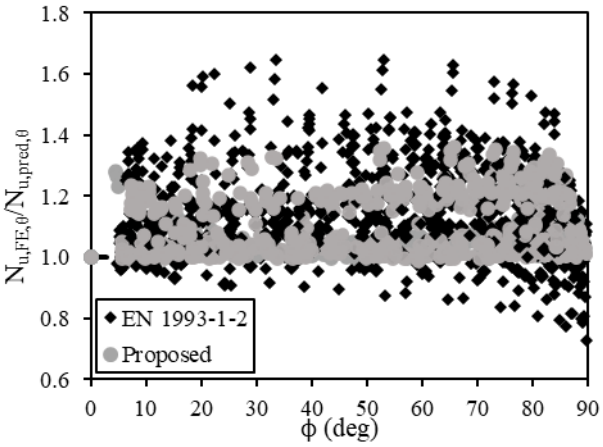

(b) RHS Duplex

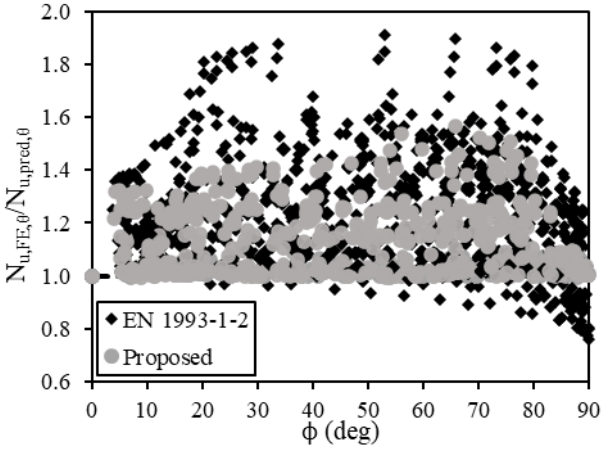

(c) RHS Ferritic

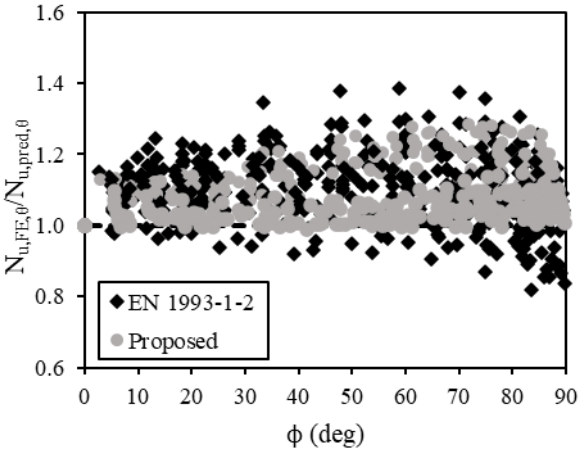

(a) CHS Austenitic

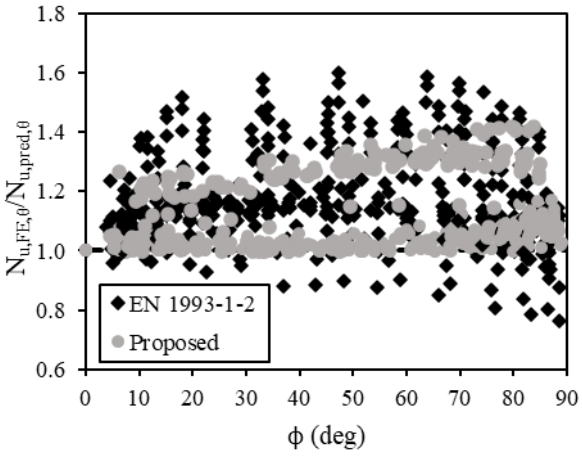

(b) CHS Duplex

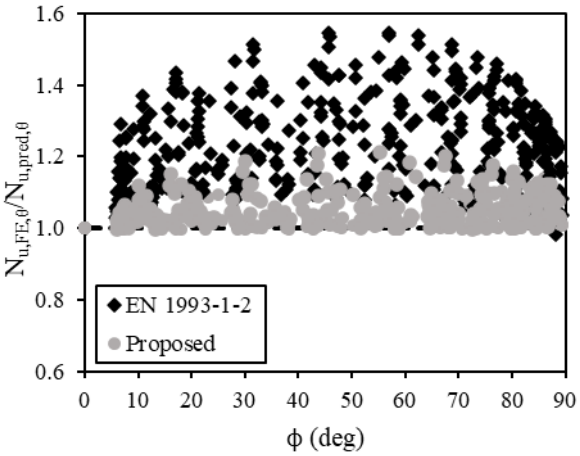

(c) CHS Ferritic

Figure 13: Comparison between the EN 1993-1-2 $N_{u,pred,\theta}$, and the proposed $N_{u,pred,\theta}$ for austenitic, duplex and ferric stainless steel beam-columns

Tables

Table 1: Room temperature stainless steel beam-column tests [25-26]

Specimen	Grade	Boundary conditions	$\bar{\lambda}$	e_y (mm)	e_z (mm)	L (mm)	$N_{u,test}$ (kN)	$\delta_{u,test}$ (mm)	$N_{u,FE}$ (kN)	$\delta_{u,FE}$ (mm)	$N_{u,test}/N_{u,FE}$	$\delta_{u,test}/\delta_{u,FE}$
SHS 60×60×3 [27]	Ferritic EN 1.4003	Pinned	0.54	10	0	774.8	199.6	7.2	203.1	7.1	0.98	1.01
			0.54	30	0	774.8	124.1	11.2	126.3	12.2	0.98	0.92
			0.54	40	0	774.8	104.7	12.0	106.7	11.8	0.98	1.02
			0.54	80	0	774.8	65.0	16.4	66.6	16.0	0.98	1.03
			0.54	125	0	774.8	46.4	18.3	47.7	18.3	0.97	1.00
RHS 100×40×2 [27]			0.56	0	2	674.8	153.2	2.7	152.3	2.9	1.01	0.95
			0.56	0	10	674.8	106.9	4.2	106.4	4.3	1.00	0.96
			0.56	0	30	674.8	62.7	5.9	63.7	6.6	0.98	0.90
			0.56	0	45	674.8	46.3	6.1	45.6	6.7	1.02	0.91
			0.56	0	75	674.8	32.0	7.4	33.9	7.9	0.94	0.94
CHS 60.5×2.8 [28]	Austenitic EN 1.4301	Pinned	1.10	5	0	1450	66.3	18.9	69.0	18.3	0.96	1.03
			1.10	15	0	1450	53.8	25.7	53.7	25.8	1.00	0.99
			1.10	25	0	1450	43.1	29.0	43.9	28.4	0.98	1.02
			1.10	40	0	1450	35.0	34.9	35.9	33.8	0.97	1.03
			1.10	85	0	1450	23.0	43.1	22.7	45.1	1.01	0.95
CHS 76.3×3 [28]			0.78	10	0	1450	94.7	16.4	99.0	16.1	0.96	1.02
			0.78	20	0	1450	79.4	19.6	81.3	19.8	0.98	0.99
			0.78	30	0	1450	66.9	22.9	69.3	23.5	0.97	0.97
			0.78	50	0	1450	50.8	26.6	52.8	25.9	0.96	1.03
			0.78	95	0	1450	34.3	38.7	34.4	36.0	1.00	1.07

Table 2: Elevated temperature stainless steel beam-colmn tests [13].

Specimen	Grade	Boundary conditions	$\bar{\lambda}$	L (mm)	e_y (mm)	N (kN)	θ_{test} (^oC)	θ_{FE} (^oC)	$\theta_{FE}/\theta_{test}$
SHS 120×120×4 [14]	Austenitic EN 1.4301	Pinned	1.05	3300	13.2	160	700.8	704.2	1.01
			1.05	3300	23.8	140	665.0	676.8	1.02

Table 3: Elevated temperature carbon steel beam-column tests [27].

Specimen	Grade	Boundary conditions	$\bar{\lambda}$	L (mm)	θ (^oC)	e_z (mm)	$N_{u,test}$ (kN)	$\delta_{u,test}$ (mm)	$N_{u,FE}$ (kN)	$\delta_{u,FE}$ (mm)	$N_{u,test}/N_{u,FE}$	$\delta_{u,test}/\delta_{u,FE}$
RHS 120×60×3.6 [29]	Carbon steel S355	Pinned	0.51	1840	400	0	242	3.36	207	3.02	1.17	1.11
			0.51	1840	400	10	139	3.17	140	3.09	0.99	1.03
			0.51	1840	400	50	73	8.91	75	8.31	0.97	1.07
			0.51	1840	550	0	186	3.62	195	3.94	0.95	0.92
			0.51	1840	550	10	111	2.31	102	2.65	1.09	0.87
			0.51	1840	550	50	49	7.12	54	6.84	0.91	1.04
			0.51	1840	700	0	71	7.54	68	6.58	1.04	1.15

Table 4: Proposed β and η parameters for cold-formed SHS, RHS and CHS columns.

	SHS/RHS			CHS		
	Austenitic	Duplex	Ferritic	Austenitic	Duplex	Ferritic
β	0.8	0.8	1.0	0.7	0.8	1.0
η	1.5	1.1	0.6	1.3	1.2	0.5

Table 5: Summary of the parametric study variables for derivation of combined loading interaction factors.

Section	Grade	Cross-section	h/b	Buckling axis	Temperatures (°C)	$\bar{\lambda}_\theta$
RHS	Austenitic	RHS 150×100×14	1.5	Major/Minor	200 °C, 400 °C, 600 °C and 800 °C	0.2-3.0
	Duplex	RHS 150×100×14	1.5	Major/Minor		
	Ferritic	RHS 150×100×14	1.5	Major/Minor		
CHS	Austenitic	CHS 100×8	-	-		
	Duplex	CHS 100×8	-	-		
	Ferritic	CHS 100×8	-	-		

Table 6: Proposed interaction factors for different cross-sections, material grades and elevated temperatures.

Section	Material	k_y or k_z		Temperature (°C)				
				200	400	600	800	200-800
RHS	Austenitic	k_z	D_1	1.9	2.3	2.4	2.6	2.3
			D_2	0.5	0.5	0.4	0.3	0.4
			D_3	1.6	1.6	1.6	1.5	1.6
		k_y	D_1	1.7	2.0	2.2	2.6	2.1
			D_2	0.6	0.6	0.5	0.4	0.5
			D_3	1.6	1.6	1.6	1.5	1.6
	Duplex	k_z	D_1	1.8	2.1	2.3	2.4	2.2
			D_2	0.5	0.5	0.4	0.2	0.4
			D_3	1.6	1.6	1.6	1.6	1.6
		k_y	D_1	1.8	2.1	2.2	2.4	2.1
			D_2	0.7	0.6	0.6	0.4	0.6
			D_3	1.6	1.5	1.5	1.5	1.5
	Ferritic	k_z	D_1	1.5	1.4	1.3	1.7	1.5
			D_2	0.5	0.5	0.5	0.2	0.4
			D_3	1.4	1.4	1.5	1.4	1.4
		k_y	D_1	1.3	1.3	1.2	2.0	1.5
			D_2	0.6	0.7	0.7	0.3	0.6
			D_3	1.5	1.5	1.5	1.5	1.5
CHS	Austenitic	k_y or k_z	D_1	2.3	2.7	2.9	2.5	2.6
			D_2	0.5	0.4	0.4	0.3	0.4
			D_3	1.6	1.5	1.5	1.6	1.6
	Duplex	k_y or k_z	D_1	1.7	1.9	2.1	2.2	2.0
			D_2	0.6	0.6	0.5	0.3	0.5
			D_3	1.6	1.6	1.5	1.5	1.6
	Ferritic	k_y or k_z	D_1	1.5	1.5	1.1	1.2	1.3
			D_2	0.4	0.4	0.6	0.5	0.5
			D_3	1.4	1.4	1.5	1.5	1.5

Table 7: Comparison of stainless steel RHS and CHS beam-column FE results with predicted resistances.

Section	Material	Buckling axis	Mean/ COV	$N_{u,\theta}/N_{u,pred,\theta}$	
				EN 1993-1-2	Proposed
RHS	Austenitic	Major	Mean	1.14	1.11
			COV	0.09	0.06
		Minor	Mean	1.09	1.08
			COV	0.08	0.06
	Duplex	Major	Mean	1.22	1.11
			COV	0.09	0.06
		Minor	Mean	1.10	1.06
			COV	0.08	0.05
	Ferritic	Major	Mean	1.33	1.15
			COV	0.10	0.05
		Minor	Mean	1.31	1.05
			COV	0.10	0.04
CHS	Austenitic	-	Mean	1.09	1.08
			COV	0.07	0.06
	Duplex	-	Mean	1.15	1.11
			COV	0.10	0.08
	Ferritic	-	Mean	1.21	1.04
			COV	0.11	0.04

Table 8: Summary of reliability assessment results.

Section	Material	Criterion	EN 1993-1-2 [9]		Proposed method	
RHS	Austenitic	Criterion 1	1.82%	Fail	0.00%	Pass
		Criterion 2	18.25%	Fail	11.27%	Pass
		Criterion 3	-8.97%	Pass	-8.67%	Pass
	Duplex	Criterion 1	1.59%	Fail	0.00%	Pass
		Criterion 2	17.47%	Pass	8.09%	Pass
		Criterion 3	-9.89%	Pass	-7.20%	Pass
	Ferritic	Criterion 1	1.82%	Fail	0.00%	Pass
		Criterion 2	11.47%	Fail	10.07%	Pass
		Criterion 3	-18.12%	Pass	-8.34%	Pass
CHS	Austenitic	Criterion 1	1.36%	Fail	0.00%	Pass
		Criterion 2	19.48%	Pass	7.95%	Pass
		Criterion 3	-8.32%	Pass	-8.00%	Pass
	Duplex	Criterion 1	1.59%	Fail	0.00%	Pass
		Criterion 2	14.59%	Pass	9.93%	Pass
		Criterion 3	-13.87%	Pass	-9.69%	Pass
	Ferritic	Criterion 1	0.00%	Pass	0.00%	Pass
		Criterion 2	4.77%	Pass	11.25%	Pass
		Criterion 3	-17.45%	Pass	-4.24%	Pass